PALEOTSUNAMI RECORD OF LARGE OFFSHORE EARTHQUAKES NORTH OF PUERTO RICO AND THE U.S. VIRGIN ISLANDS

Final Technical Report

Research supported by the U.S. Geological Survey (USGS),
Department of the Interior, under USGS award G12AP20000

Principal Investigator:
Martitia P. Tuttle
M. Tuttle & Associates
P.O. Box 345
Georgetown, ME 04548
Tel: 207-371-2007
E-mail: mptuttle@earthlink.net
URL: http://www.mptuttle.com

Project Period: 1/1/2014-6/30/2014

Program Element III: Research on Earthquake Occurrence, Physics, Effects, Impacts, and Risk
Program Element I: National and Regional Earthquake Hazards Assessments

Key Words: Paleoseismology, Tsunami Geology, Age Dating

PALEOTSUNAMI RECORD OF LARGE OFFSHORE EARTHQUAKES NORTH OF PUERTO RICO AND THE U.S. VIRGIN ISLANDS

Martitia P. Tuttle (PI), Zamara Fuentes[1], and Wilford Schmidt[2]
M. Tuttle & Associates
P.O. Box 345
Georgetown, ME 04548
Tel: 207-371-2007
E-mail: mptuttle@earthlink.net

ABSTRACT

As many as seven unusual overwash deposits within five coastal ponds and a mangrove on St. Thomas, U.S. Virgin Islands (USVI), are likely to be the tell-tale signs of tsunamis. The estimated ages and locations of the deposits suggest that the tsunamis originated from different offshore sources of large earthquakes. These deposits were found during a reconnaissance-level study and follow-on site investigations on St. Thomas and adjacent cays located near the eastern end of the Greater Antilles volcanic arc, 60 km east of Puerto Rico, and 150 km south of the Puerto Rico trench. The study sites occur within the narrow coastal zone in an otherwise high-relief setting. The unusual deposits, similar to other known tsunami deposits and distinct from the rest of the pond sediment, including other overwash deposits probably due to storms, are composed of mixed lithic and carbonate sands, hypersaline and marine shells, contain coral boulders and fragments, exhibit erosional or sharp basal contacts and, in some cases, are capped by mud. Barrier bars that front the ponds and mangrove are ~2 m above mean sea level, composed of mixed composition sand as well as cobble-size coral and lithic fragments, and were a sediment source of overwash deposits. Criteria used to identify tsunami deposits include mixed composition of sediment derived from multiple environments, presence of broken shells, microbial mat fragments, mixed or disturbed sediment, and a substantial change in environment of deposition. Advances made during this study include the following: 1) identification of overwash deposits likely to be related to the A.D. 1867 tsunami originating in the Anegada Passage; 2) identification of overwash deposits likely related to the A.D. 1650-1800 and A.D. 1200-1480 tsunamis previously recognized on Anegada, 85 km northeast of St. Thomas; and 3) identification of older overwash deposits possibly related to four tsunamis between A.D. 800-3000 B.C. One of those events occurred between 1628-393 B.C. and may have been similar to the A.D. 1200-1480 tsunami thought to have originated in the Puerto Rico trench. Additional dating of likely tsunami deposits in coastal ponds as well as documentation of coral heads and other large clasts that may have been transported onshore and deposited at higher elevations than the ponds would increase confidence in the tsunami interpretation and correlation of deposits across the island and the region. Further study on St. Thomas and other nearby islands will likely reveal a more complete record of tsunamis that will help to assess the earthquake and tsunami potential of the PRT as well as other earthquake sources in the region.

---

[1] The work reported here was done in collaboration with M. Tuttle by Z. Fuentes as part of her Ph.D. dissertation at University of Puerto Rico, Mayagüez. See Bibliography of Related Publications.

[2] Department of Marine Sciences, University of Puerto Rico, Mayagüez P.O. Box 9000 Mayagüez, Puerto Rico, 00681

INTRODUCTION

Puerto Rico and the U.S. Virgin Islands (PRVI) are located within a diffuse and complex boundary zone between the North America and Caribbean tectonic plates (Figure 1). The North America plate is moving west-southwest relative to the Caribbean plate at a rate of 19.4 mm/yr (e.g., Jansma et al., 2000; Lopez, 2006). Motion along the northern portion of the plate boundary is left-lateral strike-slip, with varying amounts of transpression and transtension (e.g., Sykes et al., 1982; Mann et al., 1990; Deng and Sykes, 1995; Mann et al., 2002). PRVI appear to comprise a microplate that is bounded by the Puerto Rico Trench (PRT) to the north, the Muertos Trough to the south, the Anegada Passage to the east, and the Mona Passage to the west (Figure 1; e.g., Masson and Scanlon, 1991; Dixon et al., 1998; Lopez et al., 1999). Side-scan sonar imagery, single-channel seismic data, and GPS geodetic measurements indicate extensive normal faulting of the carbonate platform in the central and western portion of the Mona Passage, reflecting differential eastward relative motion of the PRVI and Hispaniola microplates (e.g., Van Gestel et al., 1998; Lopez et al., 1999; Jansma et al., 2000).

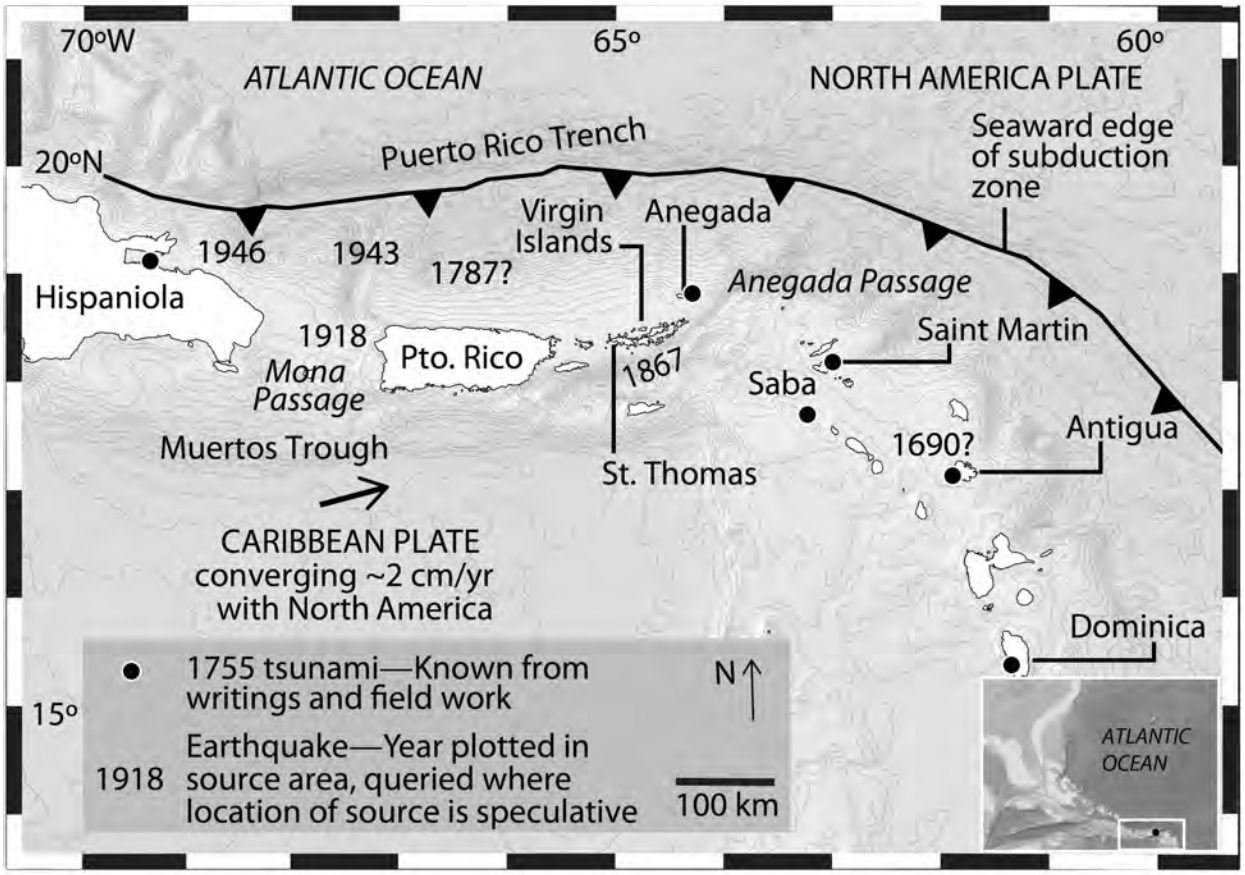

Figure 1. Regional map showing years and approximate locations of historic earthquakes, plate convergence (barbed line), direction and rate (arrow), and sightings or sediment record of the 1755 Lisbon tsunami (filled circles). Depth contour interval = 500 km. Modified from Atwater et al. (2010).

The PRVI, with a population of about 3.58 million in 2016, have a long history of destructive earthquakes, including a moment magnitude, **M** ~7.7 event in 1943 located northwest of Puerto Rico, a **M** ~7.5 event in 1918 centered in the Mona Passage, a **M** ~7.3 event in 1867 in the Anegada Passage, a **M** ~6.9-8.25 event in 1787 north of Puerto Rico and possibly related to rupture of the Puerto Rico subduction zone, and a **M** ~6 event in 1670 in western Puerto Rico (e.g., Reid and Taber, 1919; McCann, 1985; Mueller et al., 2003; Prentice and Mann, 2005; Figure 1). The locations and magnitudes of the historical earthquakes, especially the offshore events, are poorly constrained and earthquake recurrence rates are essentially unknown. The 1867 Anegada Passage and 1918 Mona Passage events are known to have produced tsunamis that inundated the coasts of PRVI (Figure 1) (Reid and Taber, 1919; Zahibo et al., 2003).

Following the devastating 2004 **M** 9.1 Sumatran-Andaman and 2011 **M** 9.0 Tohoku events, concerns about future subduction zone earthquakes and related tsunamis were heightened. Studies were initiated around the world to search for paleotsunami deposits similar to those beneath the coastal plains of Sumatra, Indonesia, and Sendai, Japan, that recorded great prehistoric earthquakes and provided clues to the earthquake potential of offshore sources (e.g., Minoura et al., 2001; Jankaew et al., 2008; Namegaya and Satake, 2014). Following the 2004 Sumatran-Andaman earthquake, the Puerto PRT was identified as a possible source of great earthquakes that could endanger northeastern Caribbean islands and perhaps the U.S. Atlantic coast (Atlantic and Gulf of Mexico Tsunami Hazard Assessment Group, 2008; ten Brink et al., 2014). A tsunami geology study on Anegada, British Virgin Islands (BVI), the closest island to the PRT, ensued. Extensive fieldwork by a diverse group of geoscientists documented and described both storm and tsunami deposits. A sand and shell layer that extends 1.5 km southward from breached beach ridges and an inland field of limestone cobbles and boulders, both dated to A.D. 1650-1800, are attributed to the 1755 Lisbon tsunami (Atwater et al., 2010). A follow up study on Anegada identified areas of reworked coral-head colonies up to 800 m inland from the northern shore and dated them to A.D. 1200-1480 (age estimate range based on 2-sigma maximum and minimum constraining ages). The "medieval" event was attributed to a near-field source on the outer rise of the PRT (Atwater et al., 2017; Wei et al., 2012).

This study, involving reconnaissance followed by detailed investigations of several coastal sites on St. Thomas, USVI, located between Anegada and Puerto Rico, explores the possibility that paleotsunami deposits on Anegada also can be recognized on other northeastern Caribbean islands (Figures 1 and 2). As reported here, sand-shell layers similar in age to paleotsunami deposits on Anegada and sharing sedimentological characteristics with modern tsunami deposits occur in coastal ponds on St. Thomas and adjacent cays or islets. If they are related to the paleotsunami deposits on Anegada, the St. Thomas deposits attest to the regional impact of the tsunamis and will help to constrain the source models of the causative earthquakes. Also, the coastal ponds on St. Thomas provide a longer sediment record than is available on Anegada and suggests at least two tsunamis prior to A.D. 1200. Results of this study indicate that a record of past tsunamis may indeed be preserved in coastal ponds of other northeastern Caribbean islands and that additional investigations on St. Thomas and other nearby islands would help to improve understanding of the earthquake potential of offshore sources some associated with the PRT and subduction zone.

Historical Earthquakes, Tsunamis, and Hurricanes

As mentioned above, several large historical offshore earthquakes caused strong ground shaking in PRVI and two of these events spawned tsunamis that inundated the coasts of PRVI. For the 1867 Anegada Passage event, there were accounts of tsunami inundation at sixty-one locations from Grenada (~760 km southwest of St. Thomas) to Jamaica (~1,190 km west of St. Thomas). Wave heights varied from 0.3 m at Grenada, 6.0 m at Charlotte Amalie on St. Thomas, to 12.0 m at Water Island ~5 km south of Charlotte Amalie (https://www.ngdc.noaa.gov; Figure 2). There is a vivid account and illustration of the tsunami breaking over the English steamer *La Plata* at Water Island. For the 1918 event, there were accounts of tsunami inundation at more than twenty locations from Dominican Republic, on the island of Hispaniola to the BVI (Figure 1). Wave heights were 6.0 m along the west coast of Puerto Rico, and diminished towards the east where they were 0.45 m at Charlotte Amalie and 0.7 m at Tortola, BVI located between St. Thomas and Anegada (Figure 1) (https://www.ngdc.noaa.gov).

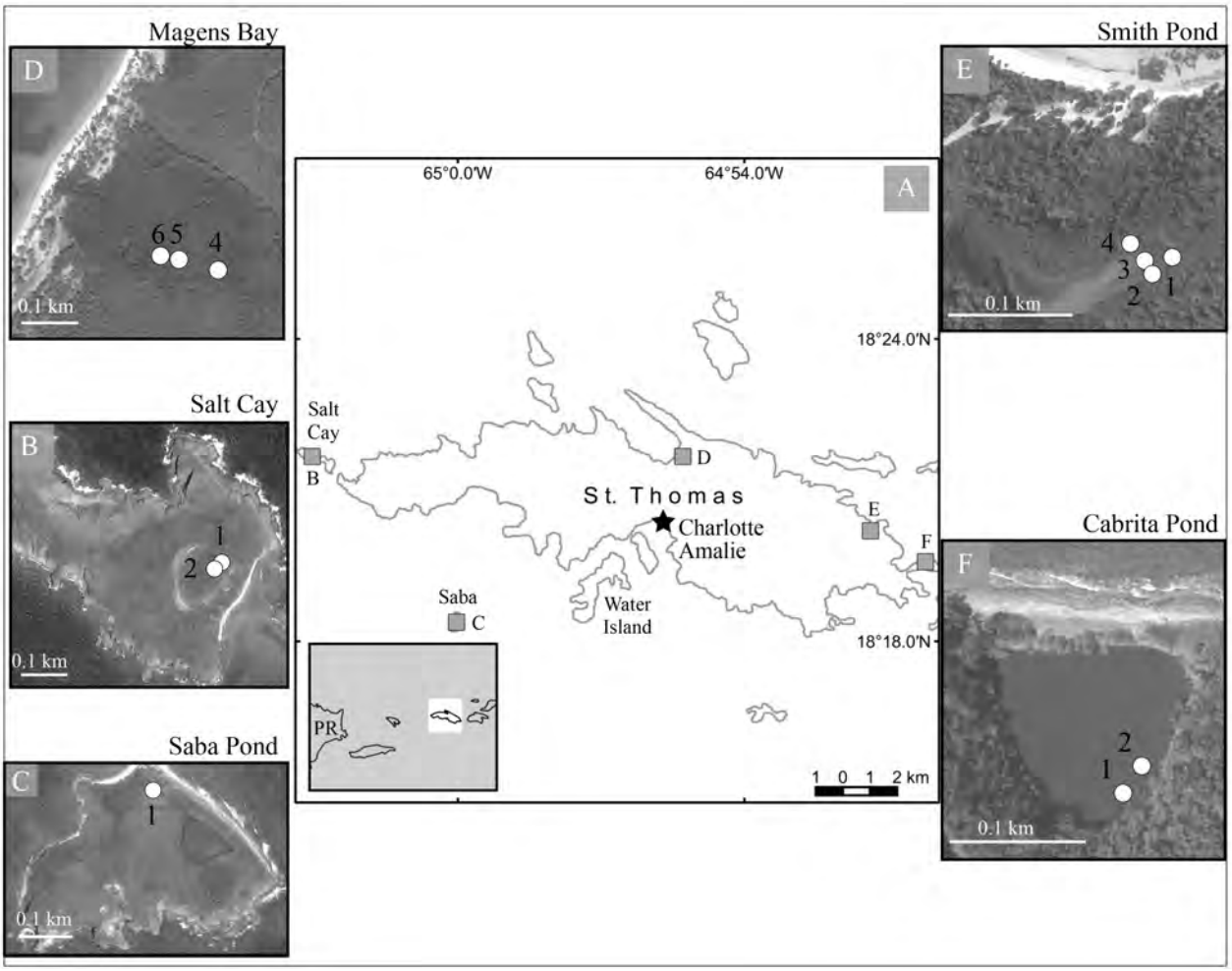

Figure 2. A: St. Thomas and adjacent cays showing locations of sites visited during reconnaissance phase of study (squares). B-F: Google Earth images of sites showing locations of gouge cores (circles); B - Salt Cay, C - Saba Pond, D - Magens Bay, E - Smith Pond, and F - Cabrita Pond.

A far-field historical earthquake, the **M** 8.5 1755 Lisbon, Portugal, earthquake, produced a trans-Atlantic tsunami that inundated the coasts of PRVI. This tsunami was observed at seventeen locations across the northeastern Caribbean from Dominica to Hispaniola, with a maximum wave height of 6.4 m at Saba about 190 km southeast of St. Thomas (Figure 1; https://www.ngdc.noaa.gov). There are no known accounts of the 1755 tsunami at St. Thomas, but it seems likely that it washed up on St. Thomas' shores given the observations at other islands in the northeastern Caribbean. At the time of the event, St. Thomas was a crown colony under the rule of the Danish Government, but the capital was on St. Croix to the south.

Tropical storms and hurricanes that form in the eastern Atlantic and move westward across the northeastern Caribbean are a common occurrence. Since 1852, seventy-eight tropical systems have passed within 150 km of Charlotte Amalie. Sixteen of the tropical systems were classified as major hurricanes (Category 3-5), six of which passed to the west of St. Thomas, subjecting its coasts to strong winds and storm surges. Twenty-five of the tropical systems were hurricanes of Category 1-2, twelve of which passed to the west of St. Thomas (https://coast.noaa.gov/hurricanes). Coastal surges resulting from these storms vary depending on the storm's trajectory, wind field, wind speed, pressure, and storm speed. Hurricanes Hugo and Marilyn are two modern hurricanes that caused storm surge at St. Thomas. In 1989, the eye of Hurricane Hugo, a category 4, passed 55 km west of Charlotte Amalie, where a NOAA tide gauge measure a water level of 0.594 m above Mean High High Water (MHHW) (https://tidesandcurrents.noaa.gov/). In 1995, Hurricane Marilyn's eye, a category 2, passed northwest of the island 10 km from Charlotte Amalie, where the same tide station registered 0.744 m above MHHW. The storm surges for these two hurricanes were much less than the 6 m wave height reported for the 1867 tsunami at Charlotte Amalie.

Tsunami versus Storm Deposits

Tsunami and storm deposits both result from onshore transport of nearshore sediment and therefore share some characteristics. Since storms deposits are common in the coastal sedimentary record of the Caribbean, care must be taken not to misinterpret storm deposits for tsunami deposits (Peters and Jaffe, 2010). Several studies have studied and compared modern and historical storm and tsunami deposits (Nanayama et al., 2000; Goff et al., 2004; Tuttle et al., 2004; Kortekaas and Dawson, 2007; Atwater et al., 2014). Many of the characteristics of the two types of deposits are summarized in Table 1. In general, tsunami deposits are more broadly distributed than storm deposits in their landward extent and height above sea level as well as their coastal extent. A recent exception is Typhoon Haiyan in 2013 that exceeded the expected landward extent and runup heights (Pilarczyk et al., 2016, Soria et al., 2016). In addition, tsunami deposits are usually composed of only a few, massive or graded layers; whereas, storm deposits often exhibit abundant stratification (e.g., Tuttle et al., 2004; Atwater et al., 2014). In differentiating tsunami from storm deposits all these characteristics must be taken into account; however, local context of the deposits also must be considered. For example, on steep-sided volcanic islands in the tropics, relatively thin tsunami deposits composed of shell and sand layers are likely to be limited to salt ponds where bioturbation is minimal; in other coastal environments, they are likely to be destroyed by erosion and bioturbation. Tsunami deposits of large clasts such as coral heads and limestone fragments are not subject to bioturbation and erosion, and therefore, serve to delineate minimum landward extents and runup heights (Atwater et al., 2017).

Previous Relevant Studies in the Northeastern Caribbean

The search for paleotsunami deposits began on Anegada, BVI in 2008 and involved several weeks of fieldwork almost every winter until 2015. The studies on Anegada, uncovered significant overwash deposits attributed to two tsunamis that occurred between A.D. 1650-1800 and A.D. 1200-1480. The two tsunami deposits differ from one another. The A.D. 1650-1800 deposit is characterized by a sand-and shell-layer within salt ponds that extends from breached beach ridges along the northern coast for 1.5 km inland (Atwater et al., 2010). The taphonomy of *Homotrema rubrum* (encrusting pink foraminfera found within the sand sheet) and sediment larger than 2 mm suggests a northern provenance (Pilarczyk and Reinhardt, 2011, Reinhardt et al., 2012). Also, the presence of autochthonous articulated shells and *Homotrema* sand in an extensive sheet-like deposit are indicative of a tsunami origin while the absence of allochthonous shells suggests a tsunami that was not strong enough to transport reef-shells over the 2.2-m high dunes (Reinhardt et al., 2012). In contrast, the A.D. 1200-1480 deposit is characterized by fields of coral-head colonies, no fewer than 200, and limestone cobbles and fragments scattered hundreds of meters inland and four meters above sea level on the Pleistocene platform (Atwater et al., 2017).

In 2010, Hurricane Earl (about category 4 at closest approach) passed 30 km to the north of Anegada (Cangialosi, 2011). Its effects on Anegada's coastal geology included deposition of wrack lines along the shores and fringes of salt ponds, accretion of small washover fans on the south shore, and deposition of microbial mat detritus along the edges and within salt ponds. Furthermore, Earl's surge on a storm berm on the north coast reworked some of the clasts of the lower part of the berm and moved a few smaller clasts a short distance inland (Spiske and Halley, 2014). While most of the main berm appeared to have initially formed by a hurricane-induced storm surge stronger than the one produced by Earl, the historic record does not include such an event. Therefore, the stronger storm is thought to pre-date the historic record. Nevertheless, the affects of the stronger pre-historic storm as well as Hurricanes Earl and Donna in 1960 (also about Category 4 when in proximity to Anegada) fall far short of the large scours and extensive deposits caused by the A.D. 1650-1800 and the A.D. 1200-1480 events.

Studies on islands south of Anegada, including Puerto Rico, Vieques, Culebrita, and USVI, also found overwash deposits that, in some cases, have been dated to specific storms or tsunamis. A reconnaissance study in Puerto Rico that involved coring of coastal ponds found sand layers composed of Halimeda (calcareous macroalgae), shells, and heavy minerals interpreted to have been deposited by the 1918 Mona Passage tsunami (Morton et al., 2006; Moya and Mercado, 2006). At the same site, two deeper sand layers containing Halimeda interpreted to be tsunami deposits date to A.D. 1270-1410 and 820-400 B.C. On Vieques and Culebrita, islands east of Puerto Rico, all sandy overwash deposits found in coastal lagoons were interpreted as storm deposits, except for the uppermost layer, which was suspected to be a tsunami deposit since it was similar in age to the historical tsunami of 1867 (Donnelly, 2005; Woodruff et al., 2008). In a recent study of human influences on sedimentation patterns on St. John east of St. Thomas, sand layers with high levels of Ca and Sr indicating a marine source were found in cores of pond sediment (Brooks et al., 2015). Some of the sand layers appear to correlate with historical storms.

Table 1. Characteristics of tsunami and storm deposits

Physical Criteria	Tsunami	Storm
Sorting	Moderately-well sorted[1] and poorly sorted[3]	Poor to well sorted[1] and well sorted[3]
Grading	Normal grading[1],[2]	Normal or inverse grading[1]
Bed thickness	Rarely more than 25 cm[1],[2], fills topographic lows[2], usually thins landward[1] but can thicken landward locally[1]	Ranging up to 95 cm[1][2]
Landscape conformity	Conform to previous landscape[1]	Does not advance beyond macrotopography[1],[2],[6]
Sedimentary and erosional structures	Massive, single to few parallel beds[1], [2], breaches meters deep and tens of meters wide[4]	Interbedded with channels, multiple laminaset[1],[2],[6], spillover fans[2],[4], breaches swaths centimeters deep and a meter across[4]
Contacts	Severed previous vegetation[2], erosional[3]	Vegetation buried in growth position by washover deposit[2],[3]
Biota	Mixture of diatoms, but more likely to contain broken valves and benthic marine diatoms[2]	Mixture of diatoms, more brackish diatoms, not as broken[2]
Rip-up clasts	Present[1],[2],[3]	Not present[1],[3]
Areal distribution	Regional to circum-oceanic[2],[4]	Regional or linear storm track [2][4][6]
Inland extent	>1 km[4],[9]	Tens of meters[2],[4], hundreds of meters[6,10]
Height above mean sea level	>4-10 m[2],[7] [8]	~1-2 m[2],[4], >6m localized[6]

Note: References in superscript brackets: 1-Goff et al., 2004; 2-Tuttle et al., 2004; 3-Morton et al., 2007; 4-Atwater et al., 2010; 5- Reicherter et al., 2010; 6-Goto et al., 2011; 7-Atwater et al., 2014; 8-Fukushima, 2015; 9-Nelson et al., 2015, 10-Kennedy et al., 2016.

STUDY SITES AND METHODS

During site visits conducting during the reconnaissance phase of the project, site characteristics were noted, including coastal energy level, surrounding slope and vegetation, height of beach berms and their composition. The tidal range at the sites is ~0.2 m (https://tidesandcurrents.noaa.gov). Each berm height was measured relative to sea level using a clinometer and tape measure. The day and time were recorded and measurements were later corrected with research quality hourly data obtained from Charlotte Amalie tide station (ID# 9751639) at http://uhslc.soest.hawaii.edu/data/?rq.

At the study sites, pond-bottom sediment was cored using a 1-m-long, 2.5-cm-diameter gouge corer. Sediment was photographed, described and sampled for datable plant material such as leaves and twigs. Beta Analytic, Inc. dated selected samples using accelerator mass spectrometry

to determine conventional radiocarbon ages in years B.P. (or before A.D. 1950). Ages were further calibrated using Calib 7.1 (Stuvier et al., 2017) and the resulting two-sigma calibrated dates are used in this report. Characteristics of storm and tsunami deposits documented elsewhere were considered in analyzing the likely origin of overwash sediment recovered in the cores (Table 1).

During more detailed site investigations conducted during the second phase of the project, beach-pond profiles were measured, sediment cores collected, laboratory analyses performed on the cores and subsamples collected in the laboratory, and stratigraphy of the cored sediment characterized. Methods used in the investigations are described below.

Topographic Profiles

During detailed site investigations, topographic profiles were measured roughly perpendicular to the shoreline and across the ponds using a Sokkia B40 automatic level mounted on an aluminum tripod and a 3.96 m leveling rod. Surveys extended from the nearshore across the barrier-beach bar and salt pond to the inland hillslope. The vertical closing error of the surveys ranged from 0.6 to 11.5 cm. The ocean water level available from Charlotte-Amalie tidal observation station (Station # 9751639) was used to provide vertical control for the surveys. The Coastal Engineering Research Center suggests that for this approach the level of uncertainty can be as much as 15.24 cm depending on the sites proximity to the tidal monitoring station. In the case of St. Thomas, distances from the tidal monitoring station to the study sites are relatively small, ranging from 3 to 15 kilometers.

Coring

At all three ponds, cores of pond-bottom sediment were collected at two to three locations along the surveyed profiles. Manual coring was performed from a wooden platform that was secured between two kayaks. Three coring systems, the Griffith, Bolivia, and Livingstone corers, were used to retrieve and to conserve pond-bottom sediment (Wright, 1967; Wright, 1991). The main differences between the coring devices are their depth capability and the diameter of the coring barrel. All three corers conserve samples for laboratory analyses. The Bolivia and Griffith corers allow the collection of 7-cm-diameter cores in polycarbonate tubes up to 1.5 m long; whereas, the Livingstone uses a 5-cm-diameter steel tube from which the core must be extruded in the field before another core can be collected. The Livingstone cores were extruded into acrylonitrile butadiene styrene (ABS) tubes. Cores from the sediment surface were collected with a Griffith corer as not to disturb the sediment-water interface. The Bolivia-Livingstone push-piston corer was used to collect deeper cores until refusal.

Laboratory Analyses

Following fieldwork, cores were shipped to LacCore, an NSF-funded national core repository, at the University of Minnesota. As part of the initial core description process (ICD), cores were logged using a GEOTEK multi-sensor core logger (MSCL) and an XYZ point sensor. Cores were later split, imaged using a GEOTEK Geoscan-III, and sediment was microscopically described using smear slides (Kelts, 2003; Schnurrenberger et al., 2003). Representative units were sampled for further analytical examination including grain-size analysis and Loss on

ignition (LOI). Sediment was pre-treated with H_2O_2 to oxidize and remove the organic matter and later run through the Horiba LA-920 grain-size analyzer (Sperazza et al., 2004). The Horiba grain-size analyzer used a refractive index of 116a001i and a size range of 0.02-2000 um. LOI was performed at temperature steps of 100°C, 550°C and 1000°C to measure carbon content in sediment samples (Heiri et al., 2001). In addition, organic samples were collected and sent to Beta Analytic, Inc. for AMS radiocarbon age determination. Radiocarbon ages were calibrated using Calib 7.1 (Stuvier et al., 2017) and the resulting two-sigma calibrated dates are used in this report.

Stratigraphic Characterization

Lithologic and biologic characteristics, including color, composition, grading and contacts with adjacent units, thickness, integrity of shells and grains, and biological assemblages were used to identify depositional units (Schnurrenberger et al., 2003). Stratigraphic units were given a letter-number code: letter referred to pond name while unit number referred to order of deposition (*e.g.*, C-1 (Cabrita-first deposited, thus oldest unit). Overwash deposits were identified by a capitalized letter-uncapitalized letter code: capitalized letters referred to pond name while uncapitalized letters were assigned alphabetically from oldest (e.g., C-a) to youngest (e.g., C-c) deposit. Radiocarbon dating of samples above, below, and within units provided age estimates for stratigraphic units and overwash deposits.

RECONNAISSANCE

During the reconnaissance phase of this project, sites were visited based on their location with respect to historical tsunamis and hurricanes, the potential to trap and preserve sediment, and low anthropogenic disturbance. Four coastal ponds and one mangrove area were investigated and are described below (Figure 2). Two of the ponds are located at Saba and Salt Cay islets, south and west of St. Thomas, respectively. The other two ponds, Smith Pond and Cabrita Pond, and a mangrove area at the head of Magens Bay, are located along the northern coast of St. Thomas.

Salt Cay Pond

The pond, located on the eastern side of Salt Cay, is fronted by a 2-meter-high barrier bar composed of coral and lithic cobbles and otherwise rimmed by vegetation (Figure 2B, 3A). Coral-rubble fans occur on the eastern interior margin of the pond. Three sandy overwash deposits (SC-a, SC-b, and SC-c) occur within the upper 1 m of otherwise muddy pond sediment (Figure 4). The lower deposit SC-a, present only at site 2, the longer core, is composed of shells, Halimeda fragments, quartz grains, lithics, and coral fragments. At sites 1 and 2, deposit SC-b is a fining upward mixture of lithics and sand with a mud cap on top. The upper deposit, SC-c located only at site 1 near the surface (~5 cm) is composed of lithic fragments and an erosional basal contact with no mud cap (See Figure S1, available in the electronic supplement of Fuentes et al., 2017). A horizontally-bedded wood fragment (SC2-W1-85) collected from a lower soil provides maximum age constraint for SC-a and SC-b, suggesting the lower unit was deposited after A.D. 690 (Table 2). A leaf (SC1-W2-28) collected from within SC-b provides a contemporaneous age of A.D. 1645-1484 for that deposit and minimum age constraint of A.D. 1645 for deposit SC-a (Figure 4). The upper layer was probably deposited within the past 300 years.

Saba Pond

Along the north coast of Saba, two ponds face northwest and northeast (Figure 2C). The western pond, protected by a coral-rubble bar and rimmed by mangroves, occurs inland from a sandy beach. The eastern pond is fronted by a 2-meter steep coral-rubble bar and no beach. At the western pond, fragments of coral species Acropora palmata, Orbicella annularis, and Diploria cavernosa occur within the tangle of mangrove roots and as part of an overwash fan that enters the pond from the north (Figure 3B). The sediment record at this pond includes two shelly overwash deposits (S-a and S-b) separated by peat (Figure 4). The lower 15 cm-thick deposit S-a is composed of carbonate fragments, clastic material, Halimeda fragments, and quartz grains.

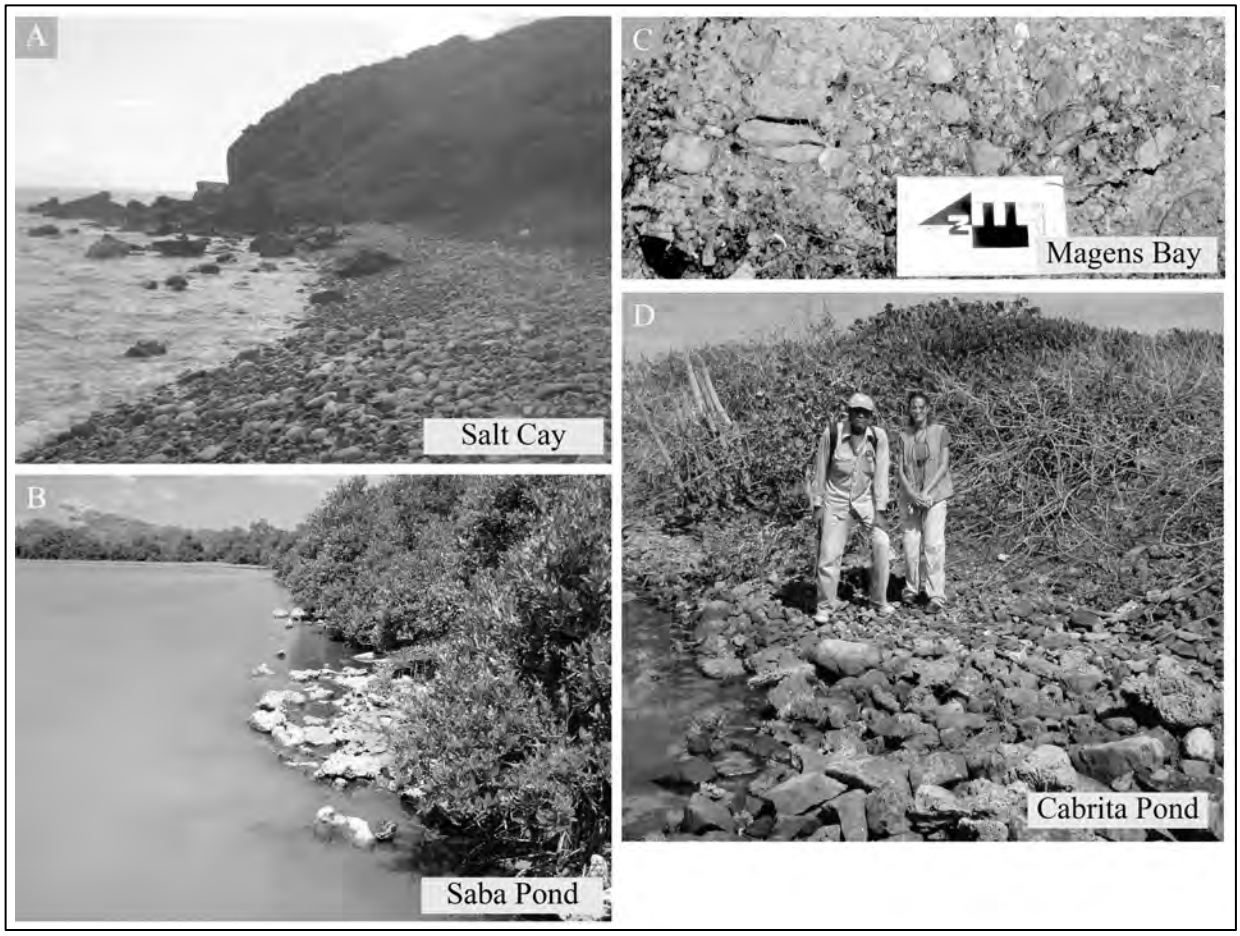

Figure 3. Barrier-bar deposits. A: Seaward portion of barrier bar at Salt Cay, view towards southwest. B: Landward portion of barrier bar fronting Saba's western pond showing coral-rubble fan deposits, view towards southwest. C: Mounds of granule- and cobble-size clasts in Magens Bay mangrove, arrow scale = 10 cm. D: Landward portion of barrier bar fronting Cabrita Pond (pond to left).

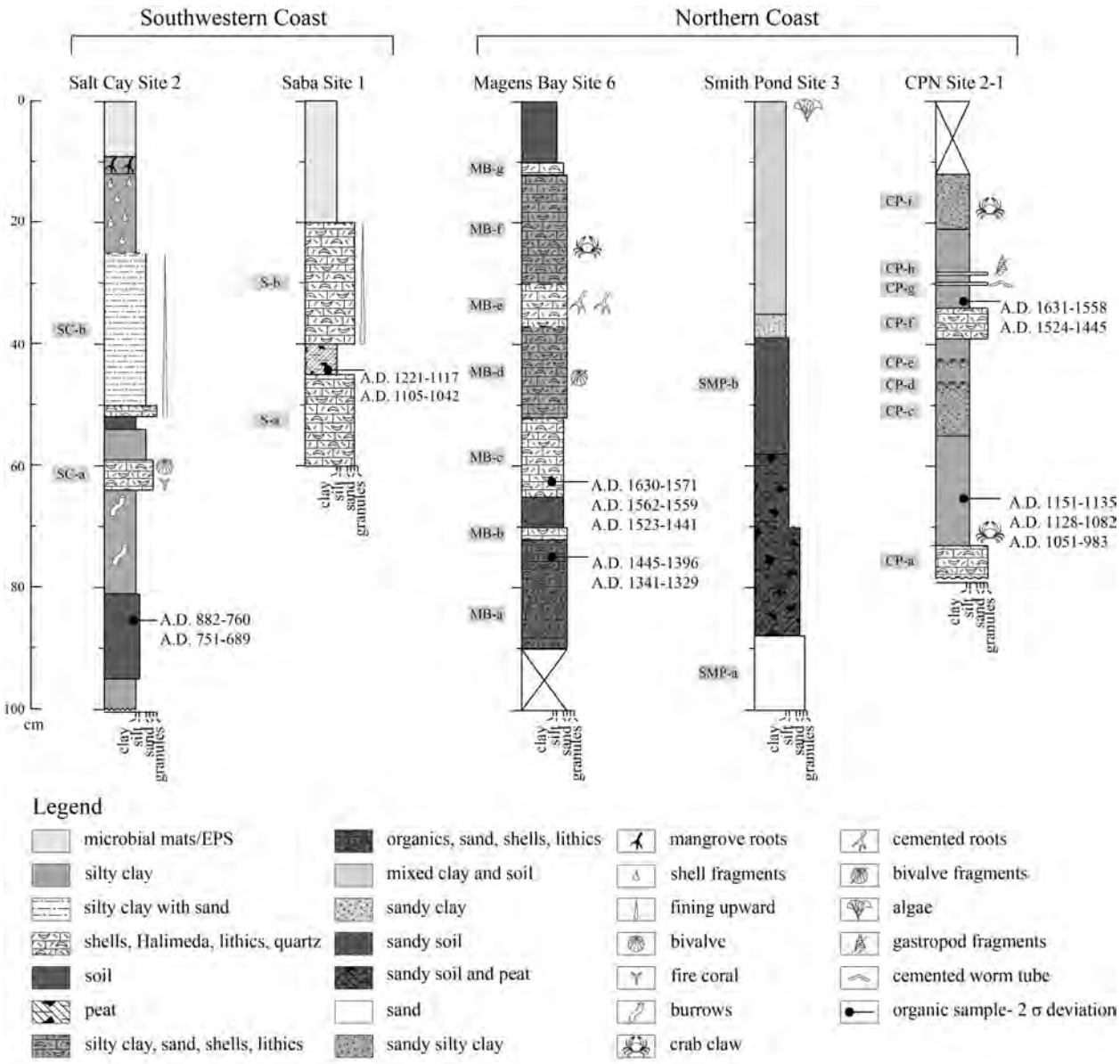

Figure 4. Representative cores showing sediment stratigraphy including overwash deposits for Salt Cay, Saba, Magens Bay, Smith and Cabrita Ponds.

The upper 20 cm-thick deposit S-b is composed of normally graded clastic material, including coarse to fine lithics, Halimeda fragments, quartz grains with an erosional basal contact. Dating of a piece of wood (SPW1-40-45) collected from the peat yielded a 2-sigma calibrated date with two ranges of A.D. 1221-1117 and A.D. 1105-1042 (Table 2), providing a minimum constraining age for S-a and a maximum constraining age for S-b. Dating suggests S-b was deposited before A.D. 1221 and S-a was deposited after A.D. 1042.

Table 2. Radiocarbon dating of samples collected on St. Thomas, USVI

Sample#-depth (cm) Lab No. (BA)*	Sample Material	$^{13}C/^{12}C$ Ratio	Conventional Radiocarbon Age (Yr B.P.)†	Calibrated Radiocarbon Dates A.D./B.C.††
SC1-W2-28 BA-319300	Leaf	-26.0	320 ± 30	A.D. 1645-1484
SC2-W1-85 BA-3255862	Wood	-24.6	1230 ± 30	A.D. 882-760 A.D. 751-689
SPW1-40-45 BA-319299	Wood	-27.4	880 ± 30	A.D. 1221-1117 A.D. 1105-1042
MB6-W1-62 BA-319298	Leaf	-27.7	390 ± 30	A.D. 1630-1571 A.D. 1562-1559 A.D 1523-1441
MB6-W2-76 BA-325861	Wood	-28.4	510 ± 30	A.D. 1445-1396 A.D. 1341-1329
CPN1-W2-28 BA-325858	Seed	-25.1	200 ± 30	A.D. 1950-1926 A.D. 1809 -1730 A.D. 1687-1647
CPN2-W1-33 BA-325859	Wood	-25.9	380 ± 30	A.D. 1631-1558 A.D. 1524-1445
CPN2-W2-66 BA-319295	Twig	-26.5	1000 ± 30	A.D. 1151-1135 A.D. 1128-1082 A.D. 1051-983
CPN2-W4-84 BA-319296	Wood	-24.8	2410 ± 30	401-548 B.C. 647-663 B.C. 688-737 B.C.

Note: For locations with one or more sites: Sample No.=(XXX#-W#) represents site code in letters followed by site number- sequence number of collected organic samples.

*Beta Analytic laboratory number.

†Conventional radiocarbon ages in years B.P. or before present (1950) determined by Beta Analytic, Inc. Errors represent 1 standard deviation statistics or 68% probability.

††Calibrated calendar dates calculated from calibrated age ranges as determined by Calib 7.1., using IntCal13 calibration dataset (Stuvier, M., Reimer, P. J., & Reimer, R. W. (2017). CALIB 7.1 [WWW program]. Ranges represent 2 standard deviation statistics or 95% probability.

Magens Bay Mangrove

Magens Bay, midway along the north coast of St. Thomas, faces northwest and is ~ 2.8 km long. At the head of the bay, there is a gently sloping 1-meter high barrier beach with a mangrove area inland of the beach (Figure 2D). In the transition area between the beach and mangrove, there are mounds of soil containing granule- and cobble-size clasts resulting from crab related bioturbation (Figure 3C). Farther inland in a ponded portion of the mangrove, silty clay sediment cored at sites 4, 5 and 6 (deepest record) include seven sand layers with varying amounts of carbonate and quartz grains, lithics, silty clay, and organic material (Figure 4; additional Figure S2 is available in the electronic supplement of Fuentes et al., 2017). At 72-90 cm below the surface, a

shelly sand in which a soil had developed, MB-a, is overlain by a couplet of sands, MB-b and MB-c, separated by sandy soil. MB-c is overlain by MB-d composed of sandy silty-clay, containing fragmented shells and lithic grains. Additionally, three sand layers occur above 38 cm, MB-e, MB-f, and MB-g, with MB-e composed of cemented clasts and root casts, while MB-f and MB-g contain articulated bivalve shells, gastropods, crab claws and shell fragments. At sites 4 and 5, sand layers, similar to site 6, are observed above 70 cm depth (Figure S2 available in the electronic supplement of Fuentes et al., 2017). Radiocarbon dating of a horizontal-bedded wood fragment (MB6-W2-76) collected from MB-a yielded a 2-sigma calibrated date with two ranges of A.D. 1445-1396 and A.D. 1341-1329 provides a contemporary age for MB-a and maximum constraining age of A.D. 1329 for MB-b (Table 2, Figure 4). Dating of a leaf (MB6-W1-62) collected near the base of MB-c provides a maximum constraining age of A.D. 1441 for MB-c and the four overlying sand layers (MB-d, MB-e, MB-f, MB-g).

Smith Pond

Smith Pond is a shallow and elongated coastal pond landward from a 1-meter gently sloping sand berm (Figure 2E). It is rimmed by mangroves and backed by a steep hill. Sediment cored at four sites (Figure 2E, see Figure S2, available in the electronic supplement to this article) contains two Halimeda layers interbedded by a mangrove peat (Figure 4). The deepest record was obtained at site 3, where a coarse sand SMP-a, observed at 86-100 cm, is overlain by a sandy mangrove peat (Figure 4). At site 1, a fine sand at 80-93 cm depth appears to correlate with SMP-a (see Figure S2, available in the electronic supplement to this article). The four sites present fine sandy clays within 39-60 cm depth and a lower bioturbated erosive contact. At site 1 cemented burrows were observed within the clay unit below the upper sandy layer. The upper section of the cores consists of gray clays that are very similar to deposits being accumulated today.

Cabrita Pond

This pond is characterized by a steep, 2- meter high coral-rubble barrier bar and is backed by a hillslope (Figure 2F, 3D). Nine sandy deposits were found interbedded with muddy sediment at coring sites 1, 2-1, and 2-2 (Figure 4). The deepest sandy deposit, CP-a, was found at sites 2-1 and 2-2, and is composed of coarse sand, worm tube fragments, bivalve and gastropod shells, cemented cerithids, quartz and feldspar grains. This deposit fines upward from granule-size shells to carbonate and lithic-rich coarse sands to mud. Deposit CP-b is a very thin sand and is only observed at site 2-2 (see Figure S3, available in the electronic supplement of Fuentes et al., 2017). Deposits CP-c to CP-e were retrieved only at sites 2-1 and 2-2. Deposit CP-c consists of sandy clay while CP-d and CP-e consist of mud containing a couplet of very thin sand layers with articulated and disarticulated bivalve shells and some cerithids. Immediately above the couplet, a thin shelly sand deposit, CP-f, present at all sites, is composed of shells, Halimeda, lithics and quartz grains. A mud cap is absent from this deposit, however, the presence of small crab claws suggests a mud cap could have been destroyed by bioturbation. Another couplet, CP-g and CP-h, composed of thin layers of gastropod fragments and cemented worm tubes, occurs higher in the section at sites 1 and 2. The ninth deposit, CP-i, occurs near the surface and is composed of a sandy silt clay and was encountered at both sites. The timing of the nine overwash deposits can be estimated broadly from radiocarbon dating of organic samples collected from the cores. For deposit CP-a, a twig (CPN2-W4-84; collected from site 2-2 and not shown on Figure

4) from within the deposit provides a maximum age of 737 B.C., while a twig (CPN2-W2-66) collected above CP-a provides a minimum constraining age of A.D. 1151 (Table 2; Figure 4). Sample CPN-W2-66 also provides a maximum constraining age of A.D. 983 for CP-b to CP-f and sample CPN2-W1-33 provides a minimum constraining age of A.D. 1631 for those deposits (Table 2). A mangrove seed (CPN1-W2-28; not shown on Figure 4) collected from mud below CP-g provides a maximum constraining age of A.D. 1647 for deposits CP-g, CP-h, and CP-i.

Interpretations

Of the numerous overwash deposits identified at the study sites, five are interpreted as tsunami deposits and six are interpreted as storm deposits. Salt Cay pond sediment contained three overwash layers, of which two are interpreted as tsunami deposits (SC-a and SC-b) and one as storm or tsunami deposit (SC-c); while at Saba Pond two overwash layers are interpreted as tsunami deposits (S-a and S-b) (Figure 4). At Magens Bay, two overwash layers are interpreted as tsunami deposits (MB a-b and MB c-g). The unit MB a-b is represented in the sediment record by two sand layers while MB c-g is represented by five. At Smith Pond, two overwash layers (SMP-a and SMP-b) are interpreted as tsunami deposits. At Cabrita Pond, two overwash layers (CP-a and CP-f) are interpreted as tsunami deposits, while seven overwash layers (CP-b-e and CP-g-i) are interpreted as storm deposits.

Considering that most of the study sites lie within the topographic range of storm surge influence, physical criteria were used to distinguish between tsunami and storm deposits (Table 1). Cored overwash layers in four (Salt Cay, Saba Pond, Magens Bay, and Cabrita Pond) out of the five sites with mixed composition (marine and lacustrine), erosional contacts, fining upward sequences, and mud cap at some sites were interpreted as tsunami deposits. Several cored overwash layers at Salt Cay and Cabrita Pond that lacked mixed composition (mostly of lacustrine composition) and had conformable contacts that were sharp but not erosive were interpreted as storm deposits. At Salt Cay, Saba, Smith, and Cabrita Ponds, environmental changes occur following overwash events consistent with tsunamis. More specifically, at Salt Cay following the deposition of SC-c, there is a change in conditions from a marine environment that sustained mangroves to a hypersaline environment where microbial mats thrived. At Saba and Smith Ponds, a mangrove forest where peat was accumulating changed to a hypersaline environment after deposition of S-b and SMP-b; while at Cabrita Pond, bivalve shells disappear after deposition of CP-f.

The most recent overwash events are recorded in Salt Cay and Cabrita Pond (Figures 5 and 6). The origin of the uppermost layer is equivocal, it has an erosional basal contact but it was only observed closest to shore and is not capped by mud. Provided it was deposited during the past 300 years; the upper layer could be related to either the 1867 tsunami or a historical storm with a significant surge.

At Cabrita Pond, a conformable contact and no mixed composition are characteristics of storm deposit for which the most likely culprits are the 1867, 1894 or 1995 hurricanes. The category 3 1867 hurricane, which had an E-W trajectory and passed north of St. Thomas two weeks before the 1867 tsunami, might not have had a substantial impact on its coasts. The category 2 1894 and 1995 hurricanes, traveling from south-southeast to north-northwest and southeast to northwest,

respectively, and passing over the western part of St. Thomas, could have had a much larger impact on the island that the 1867 hurricane.

The A.D. 1650-1800 event appears to be recorded at Salt Cay and Magens Bay while the A.D. 1200-1480 event appears at all locations (Figures 5 and 6). At Salt Cay, the lower two layers are interpreted as tsunami deposits because they occur in all three cores at the site, have mixed compositions, show normal grading, are capped by mud, and have erosional basal contacts. The two layers were deposited between A.D. 689-1645. The lower layer may have been deposited during the A.D. 1200-1480 tsunami while the middle layer may have been deposited by the 1755 tsunami, but a previously unrecognized event cannot be ruled out. At Saba, the presence of mixed material, an erosional contact and normal grading are all characteristics consistent with a tsunami origin. Dating suggests the upper layer may have been deposited during the A.D. 1200-1480 tsunami while the lower layer might be related to an earlier event also recorded at Cabrita Pond. At Magens Bay characteristics of the upper overwash deposit- varied composition, absence of a soil horizon in between the layers and distance from shore, ~330 m - suggest that it formed as the result of five waves in a tsunami wave train. Though the minimum age is unknown, the maximum constraining age is A.D. 1441 indicating that the deposit is historical and could have resulted from the 1755 Lisbon earthquake (Figure 1, 4).

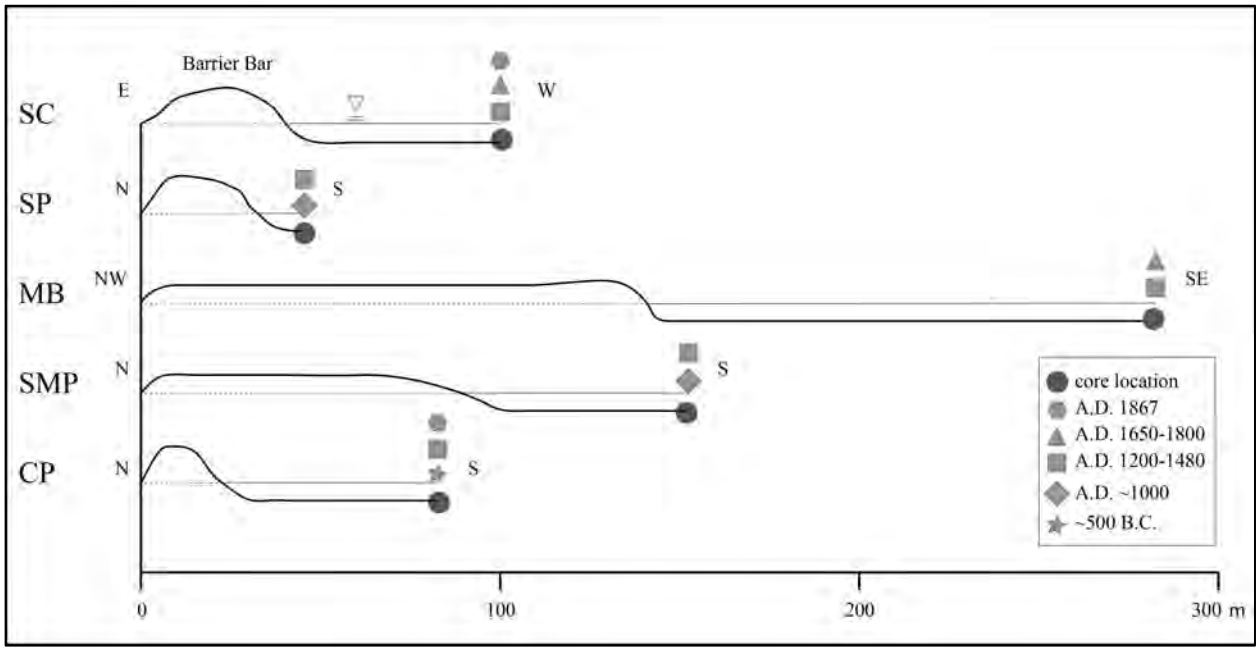

Figure 5. Beach profile sketches of study sites, showing inland distance of overwash deposits interpreted as likely related to tsunamis: SC - Salt Cay, SP - Saba Pond, MB - Magens Bay, SMP - Smith Pond, and CP-– Cabrita Pond. Distance on the x-axis is in meters.

Modeling of the 1755 tsunami in the northeastern Caribbean shows oscillation of waves within Magens Bay (Wei, pers. comm., 2012). If the multi-layer deposit is related to the 1755 tsunami, our finding would further extend the recognized distribution of tsunami deposits related to this event. Also at Magens Bay, the lower overwash deposit, separated from the upper overwash deposit by a soil, clearly represents an earlier event. A contemporary age of A.D. 1445-1329

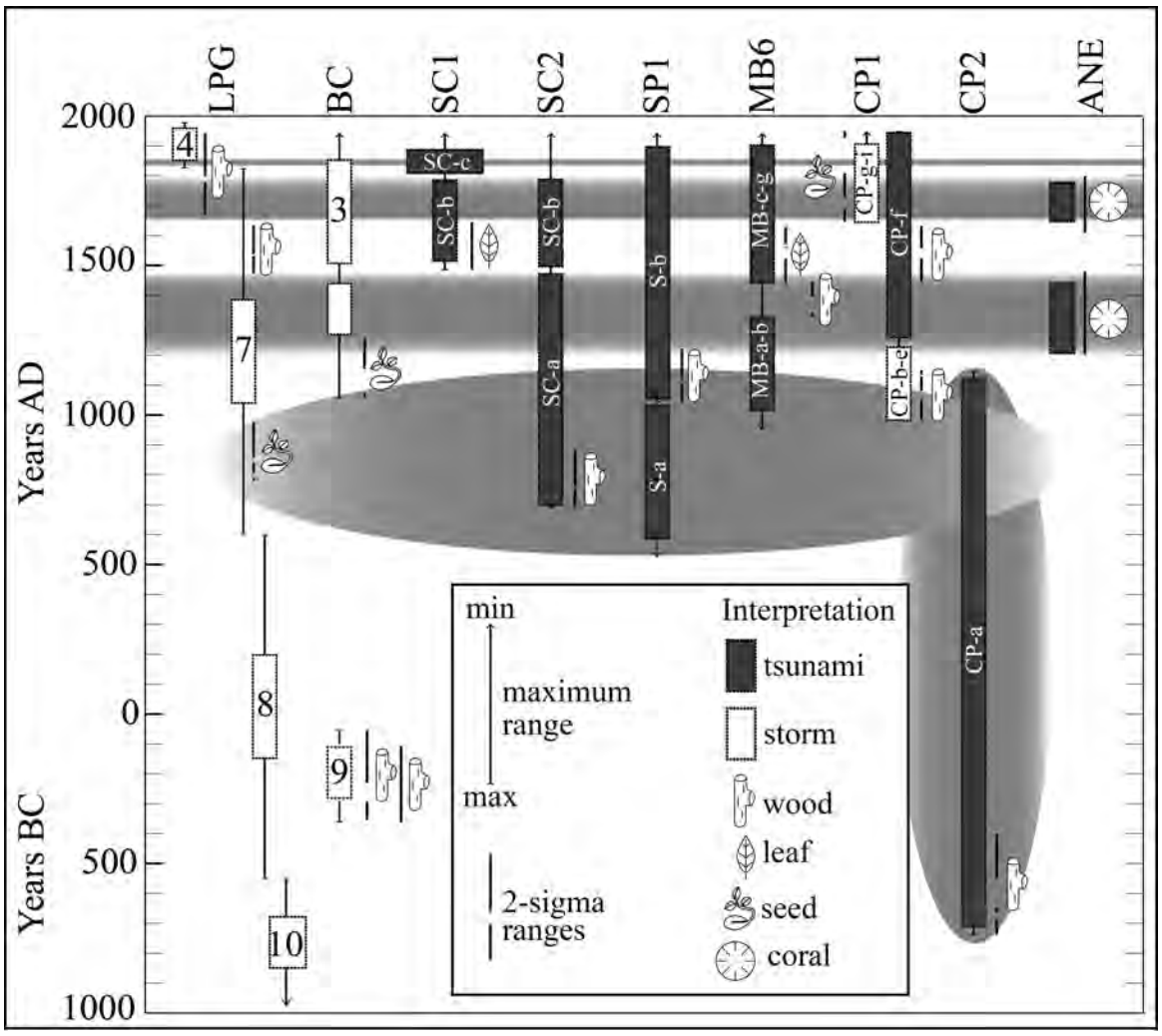

Figure 6. Regional chronology of overwash deposits generally organized from southwest on the left to northeast on the right found at the following locations: LPG - Laguna Playa Grande in Vieques, PR (Woodruff et al., 2008), BC - Big Culebrita Salt Pond in Culebra, PR (Donnelly, 2005), SC1 - Salt Cay site 1, SC2 - Salt Cay site 2, SP1 - Saba Pond site 1, MB6 - Magens Bay site 6, and CP1 - Cabrita Pond site 1, and CP2 - Cabrita Pond site 2 in St. Thomas, USVI (this report), and ANE – Anegada, BVI (Atwater et al., 2017). Horizontal bars from top to bottom denote: A.D. 1867, AD 1650-1800, and AD 1200-1480 date ranges associated with historic and interpreted pre-historic events. Gray ovals represent additional possible dates for overwash deposits identified in SP1 and CP2 during this research. Arrows indicate minimum and maximum ranges for each labeled deposit, according to organic samples obtained for that location.

suggests the deposit may be related to the A.D. 1200-1480 tsunami recognized on Anegada. Moreover, the finding would enlarge the area of impact for this event and could help model its source. At Smith Pond, while the lower overwash deposit is overlain by peat and is present at two sites, the absence of a basal contact for the sand limits our interpretation of the deposit. For the overlying sand layer, its distance (~150 m) from the coast and its erosive basal contact with underlying peat suggests a high-energy erosional event followed by deposition of sand consistent with a tsunami. In contrast, the fine-grained sediment of the upper 39-60 cm is indicative of a

prolonged period of quiet-water deposition. Unfortunately, there were no organic samples from this site that could help constrain the ages of the likely tsunami deposits; we aimed to correct this during the followup site investigation.

While there were too few radiocarbon dates to narrowly constrain the ages of the likely tsunami deposits, results of the reconnaissance phase of the study suggest that Salt Cay, Saba Pond, and Magens Bay contain tsunami deposits that fall in the A.D. 1650-1800 and the A.D. 1200-1480 range (Figure 5 and 6). For the earlier event, A.D. 1200-1480, all locations show deposits that fall within this range. At Saba Pond, the absence of a sample that provides a minimum for the upper sample causes S-b to fall within both ranges, and requires further dating to decrease the range. During this study, Cabrita and Saba ponds record tsunami deposits that occurred sometime before A.D. 1000, pointing to the possibility of an older event, possibly regional, that affected the coasts in St. Thomas and nearby cays. At Cabrita Pond the record is extended to 737 B.C. and could indicate an even older event that affected the north coast of St. Thomas. For the historic record, additional dating including Cs-137 dating is needed to compare ages of overwash deposits on the various islands.

A storm chronology based on sediment cores from one pond each on Culebrita and Vieques (Donnelly, 2005 and Woodruff, 2008) includes forty-two events over the past 5000 years interpreted from overwash deposits. Eight of those events fall within the A.D. 1200-1480 range and another eight events occurred before A.D. 600 (Figure 6). Given recent findings on Anegada and possibly St. Thomas of likely tsunami deposits related to the 1755 Lisbon event and a Medieval event associated with the PRT, some of the overwash deposits previously interpreted as storm deposits may instead be related to tsunamis.

Distance inland, coastal bathymetry, berm height, and hydrological conditions are some of the factors that appear to have influenced deposition and preservation of overwash deposits in the coastal environment of St. Thomas. The ponds that were able to trap and preserve the most overwash deposits - Salt Cay and Cabrita Ponds - had higher barrier bars and bowl-shaped bottom morphology (Figure 5). These two ponds may have remained filled with saltwater most of the year, perhaps through seawater percolation through the base of the barrier bar.

While most tsunami deposits thin landward (e.g., Morton, et al. 2007), in other cases tsunami deposits fill in topographic lows (Tuttle et al., 2004) and thicken landward (Jaffe, et al. 2006). At Cabrita Pond, the upper tsunami deposit thickens landward. We attribute this to the topography of the site, specifically the steep hillslope behind the pond, which served as a backstop and likely affected deposition. In our model, the tsunami wave traverses the beach and barrier bar eroding, suspending, and transporting sediment from the various environments, enters the pond depositing a thick layer of coarse-grained sediment across the pond bottom and especially at the back of the pond where the wave is abruptly stopped by the hillslope. Soil and sediment from the hillslope is likely to be eroded by runup and backwash and deposited along with sediment transported from other environments towards the back of the pond. Fine-grained sediment would remain suspended in the pond for a period of minutes to hours, but would eventually settle out of the water column and be deposited on top of the coarse sediment, forming a mud cap. This model is similar to that developed to explain Storegga Slide tsunami deposits in coastal ponds in western Norway, northeastern Scotland, and the Shetland Islands (Bondevik et al., 2005).

SITE INVESTIGATIONS

Based on the results of the reconnaissance phase of this study, three coastal ponds were selected for detailed investigations. The sites included Smith Pond (SMP) and Cabrita Pond North (CPN) along the northeastern coast of St. Thomas and Perseverance Pond (PERS), not visited during reconnaissance, on the southwest coast (Figure 7). Perseverance Pond was selected with the hope that it might contain a record of the 1867 tsunami known to have inundated Charlotte Amalie only 6 km east-southeast of the pond.

Smith Pond

The northern edge of Smith Pond is 143 m south of Smith Bay beach shore (Figure 7B). The Smith Pond area is underlain by the Louisenhoj Fm. of Albian age which is composed of augite-rich andesitic volcanic breccia and tuff with minor occurrences of conglomerate (Donnelly, 1966). Quaternary deposits vegetated by mangroves rim the pond. Between the pond and the barrier beach to the north, mangroves transition to forest. The barrier beach is composed of *Halimeda* sand, coral fragments, shells, and beach rock. Along the northeastern shore of Smith Bay, beach rock, sea grasses and calcareous green algae occur along with a modest amount of white carbonate sand, while the northwestern shore is composed primarily of carbonate sand. A fringing reef occurs about 130 meters north of the shoreline.

Coring

The pond measures 30 m across roughly perpendicular to the shoreline and 160 m across parallel to the shoreline. Water depth at the time of sampling was about 11 cm. During the investigation, a total of seven cores were collected at two sites along a transect with a bearing of N27.5°W (Figures 7B). Site 1 (SMP14-1A, denoted as 1a on Figure 7B) is located farthest inland about 18 m from the northern edge of the pond, while Site 2 (SMP14-2A) is located 6 m from the northern edge of the pond (Figure 7B). Three cores were collected at site 1, reaching a maximum depth of 1.5 m. Two additional overlapping cores were retrieved within a meter of site 1 (denoted as 1b in Figure 7B), reaching a maximum depth of 1.71 m. At site 2, two cores were collected, reaching a maximum depth of 1.16 m.

Stratigraphy and Chronology

At the two core sites, three main depositional units were identified based on lithostratigraphic and biostratigraphic characteristics (Figure 8). The characteristics of the units are described below, including their color, composition, integrity of shells and grains, grading, and contacts with adjacent units. At least three layers are identified as overwash deposits. Unit S-1 is present at both sites and is composed of fibrous peat overlain by medium to thick beds of bioturbated light brown to light tan coarse carbonate sands (S-a). The fibrous nature of the peat is indicative of fine lateral mangrove roots. Sand layers are composed of coarse *Halimeda* (calcareous green algae) segments, carbonate grains, foraminifera and quartz grains. The sand is similar in composition to the sand found at the beach today. At site 2, the entire observed thickness of S-1 is composed of bioturbated sand. At site 1, a layer of peat clasts divides the sand layer into two thinner layers. The lower sand layer at 127-148 cm depth is underlain by peat and the upper

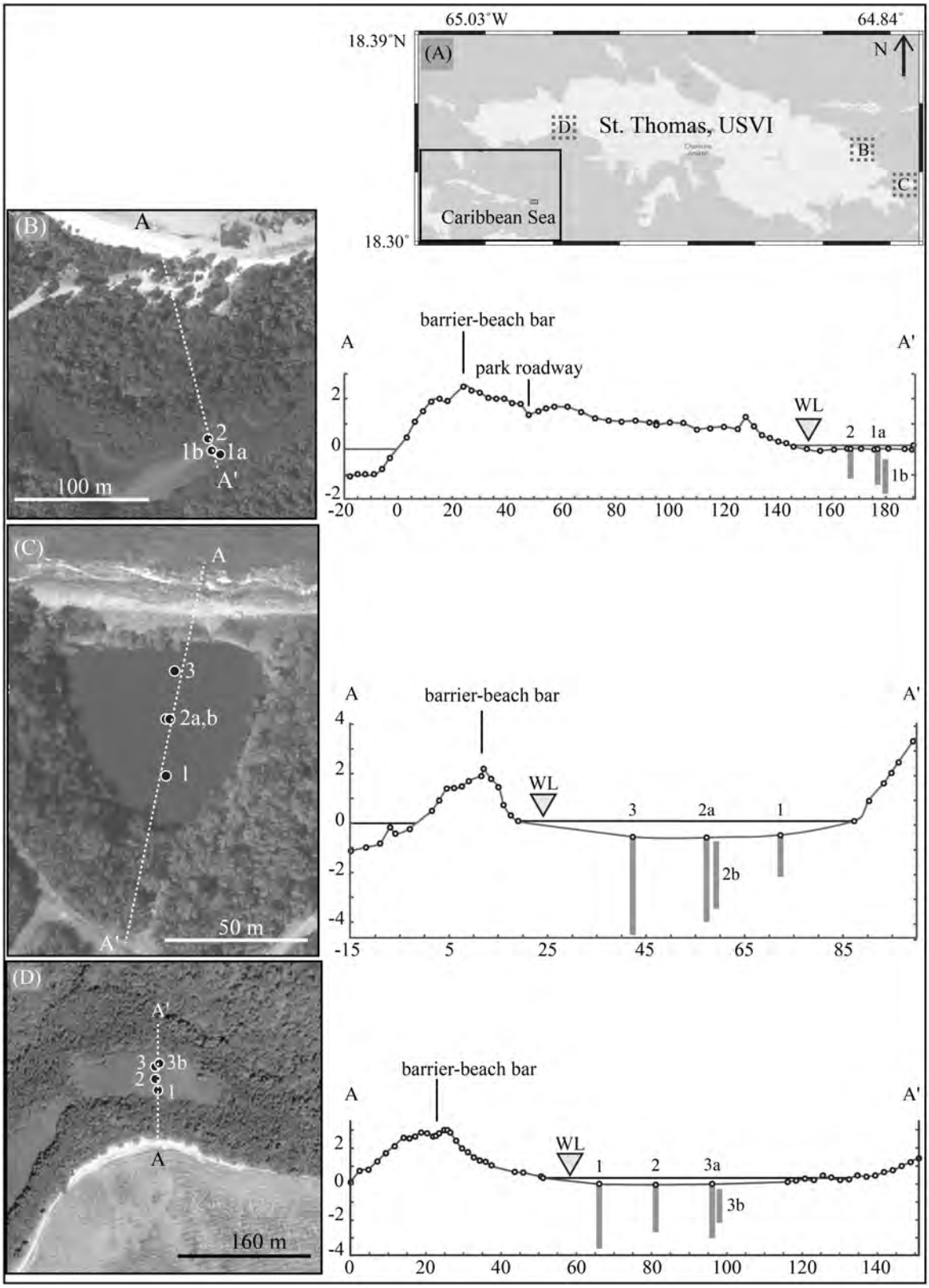

Figure 7. A: St. Thomas and adjacent cays showing locations of detailed site investigations (dashed boxes); B-Smith Pond, C-Cabrita Pond, D-Perseverance Pond. B-D: Google Earth images of sites showing transect and topographic profile (to the right) and core sites (circles).

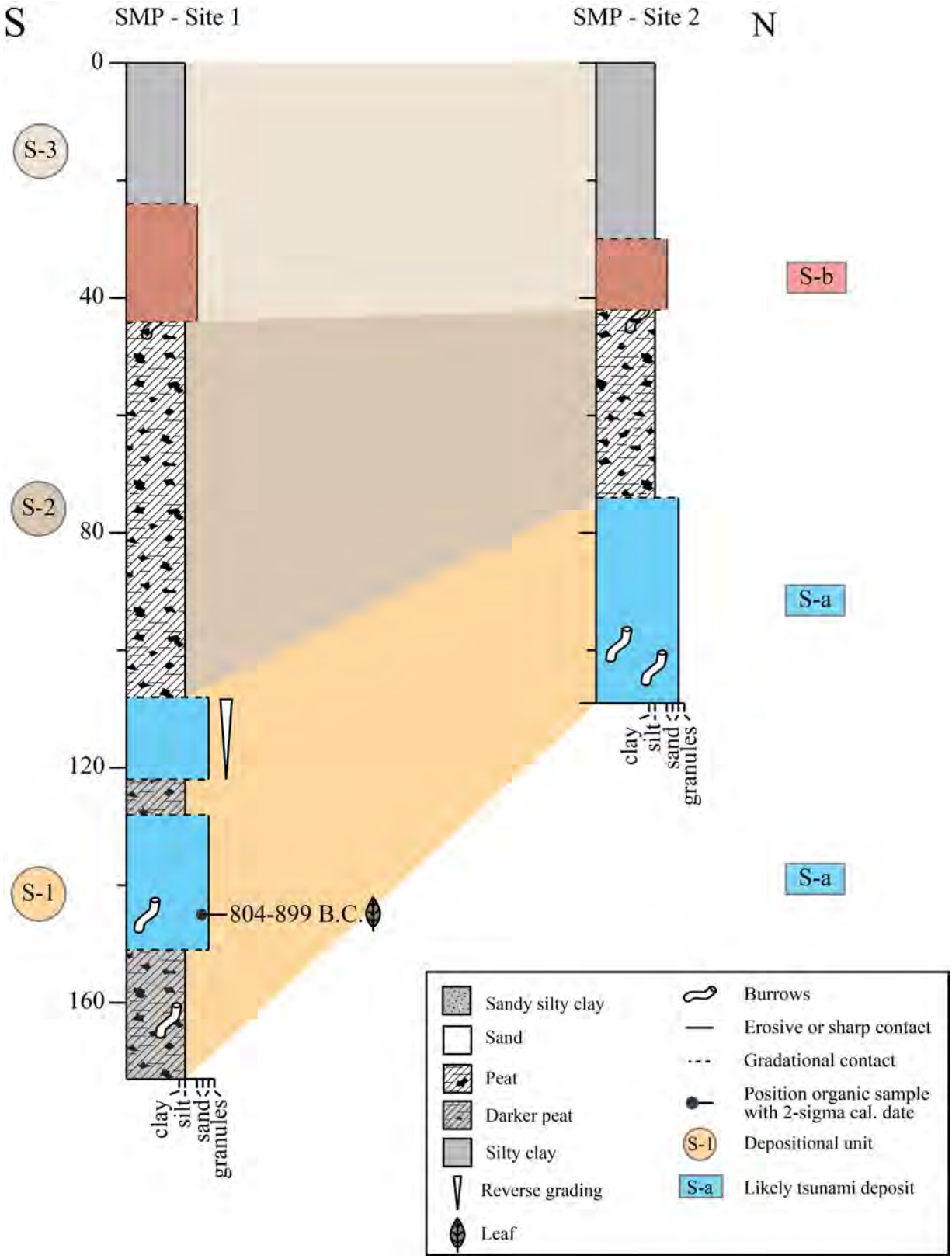

Figure 8. Core logs, radiocarbon date, and stratigraphic interpretation for Smith Pond. Cores collected along transect roughly perpendicular to the coast.

Table 3. Radiocarbon dating of samples collected on St. Thomas, USVI

Sample No.-depth (cm) Lab No. (*BA*)*	Sample Material	$^{13}C/^{12}C$ Ratio	Conventional Radiocarbon Age (Yr BP)[1]	Calib 7.1 Calibrated Calendar Date (AD/BC)[2]
Cabrita North				
1A-2B-8.5 *Beta-389594*	Twig	-25.4	2160 ± 30	351-300 B.C. 227-224 B.C. 210-168 B.C.
1A-2B-56.2 *Beta-389595*	Leaf	NA	3280 ± 30	1628-1498 B.C.
1A-2B-74.5 *Beta-389596*	Leaf	-28.1	3520 ± 30	1927-1753 B.C.
1A-2B-81.5 *Beta-389597*	Leaf	-28.9	3580 ± 30	2027-1878 B.C. 1839-1828 B.C.
2A-2B-30 Beta-389598	Leaf	NA	1940 ± 30	18-14 B.C. 0-A.D. 129
2A-3B-98 *Beta-389599*	Leaf	-26.8	3970 ± 30	2574-2451 B.C. 2419-2405 B.C. 2378-2350 B.C.
3A-5L-82-82.5 *Beta-389600*	Charcoal or leaf	NA	4350 ± 30	3080-3070 B.C. 3025-2901 B.C.
Perseverance				
2A-2L-77 *Beta-389602*	Leaf	-29.0	2380 ± 30	726-720 B.C. 703-695 B.C. 541-393 B.C.
3A-2B-35.5 *Beta-389603*	Leaf	NA	1910 ± 30	A.D. 22-145 A.D. 150-170 A.D. 194-209
Smith				
1B-2L-62 *Beta-389604*	Leaf	-26.4	2690 ± 30	899-804 B.C.

sand layer at 105-121 cm depth shows reverse grading. Most depositional structures in unit S-1 at both sites have been destroyed by bioturbation. Radiocarbon dating of a leaf (1B-2L-62) collected from the lower sandy layer at site 1 yielded a two-sigma calibrated date of 804-899 B.C.

Note: Sample No. #X-#X-# represents (coring site, hole at site – drive in hole, tool used for drive – depth of collected organic samples).

**Beta Analytic* laboratory number.

[1] Conventional radiocarbon ages in years B.P. or before present (1950) determined by Beta Analytic, Inc. Errors represent 1 standard deviation statistics or 68% probability.

[2] Calibrated calendar dates calculated from calibrated age ranges as determined by Calib 7.1 using IntCal13 calibration dataset (Stuvier, M., Reimer, P. J., & Reimer, R. W. (2017). CALIB 7.1 [WWW program]. Ranges represent 2 standard deviation statistics or 95% probability.

and provides a minimum constraining date for the underlying peat, a contemporary date for the sand layer, and a maximum constraining date for the overlying sediment (Figure 8 and Table 3).

A distinct compositional change between units S-1 and S-2 is marked by a sharp lower contact that shows signs of bioturbation. Unit S-2, present at both sites, consists of a brown bioturbated bed of sandy silty clay with significant amounts of plant material, *Halimeda* segments, multi-chambered foraminifera, and quartz grains underlain by a brown, bioturbated peat with abundant coarse *Halimeda* segments, and vertical roots that penetrate down to S-1. No overwash deposits are observed within S-2.

A sharp contact separates S-2 from S-3. Unit S-3, found at both sites, is composed of a black, massive bed of siderite clay with a light tan layer of bioturbated, sandy silty clay at the bottom that is thicker at site 1 than site 2. The lower portion of S-3 contains carbonate and quartz grains, foraminifera, and plant fragments, while the upper portion of the unit is overlain by a green algae mat. The lower part of S-3 is interpreted as an overwash deposit (S-b).

Sequence of Pond Environments

Smith Pond appears to have formed in a recess in the northeastern coast of the island. Sediment that has accumulated in the pond shows a change in deposition from an initial mangrove swamp to a coastal pond. Dating of a leaf (1B-2L-62) from the clastic layer S-a in the depositional unit S-1 suggests the pond was a mangrove swamp prior to 804 B.C. (Figure 8). About 804-899 B.C., the mangrove swamp was inundated during which a clastic layer of S-a containing an interbed of peat ripup clasts was deposited. The mangrove environment survived this event and persisted for perhaps 1.5-2 thousand years, based on the position of the layer within the section, until another event deposited a clastic layer of S-b across the swamp. The mangrove did not recover following the second event and instead became a salt-water pond. At some point, conditions developed that allowed for the growth of marine macroalgae which covers the pond surface today.

Overwash Events

Two overwash events are recognized in the sediment record of Smith pond. Sand layers S-a and S-b are interpreted as likely tsunami deposits due to the presence of *Halimeda* segments and the transport distance from the shore. In addition, S-a at site 1 contains an interbed of peat ripup clasts and exhibits reverse grading. Following the deposition of S-b, there was a dramatic change in environment from a mangrove swamp to a salt-water pond.

About 804-899 B.C., the first event deposited coarse *Halimeda* sands with an intervening layer of peat ripup clasts on top of peat that had formed in a mangrove swamp. The sand layers within S-1 are thought to be beach sediment that was entrained and transported 140 m inland and deposited in the mangrove swamp by two train waves. In addition, the first wave of the tsunami may have ripped up and entrained pieces of the peat as it entered the swamp. The peat clasts, having a relatively low specific gravity than sand, would have remained suspended while the clastic material was deposited. As the tsunami receded, the clasts settled out on top of the first sand deposit but then were buried by the second sand layer delivered to the swamp by the second wave.

Perhaps about 1.5-2 thousand years later, the second event deposited clastic sediment including *Halimeda* sands again on top of peat that had formed in a mangrove swamp. During this event, the mangrove swamp was closed off from the open bay and a salt-water pond formed which still exists today.

Cabrita Pond North

Cabrita Pond North is located on the northern shore of a peninsula that divides Muller Bay from Great Bay on the northeast side of St. Thomas (Figure 7). The pond is surrounded on its western, southern, and eastern sides by vegetated hillslopes and a Quaternary barrier bar on its northern shore (Figure 7C). The pond and surrounding slopes are underlain by the Louisenhoj Formation of Albian age (Donnelly, 1966). The barrier bar is composed of coral fragments, cobbles, and boulders that form a 2-m high beach ridge and a beach platform with coarse lithic and carbonate sand, cemented coral fragments, and lithic boulders. Offshore, the seabed is vegetated by sea grass and *Halimeda*. The pond measures 75 m across perpendicular to the shoreline and 65 m across parallel to shoreline. Water depth of the pond at the time of coring was about 63 cm and there were abundant *Cassiopea* jellyfish living on the pond bottom.

Coring

During the investigation, a total of 15 cores were collected at three sites along a transect with a bearing of N8.5°E (Figure 7C). Site 1 (CPN14-1A) is located farthest inland about 53 m from the northern edge of the pond, while site 2 (CPN14-2A) and site 3 (CPN14-3A) are located 37 and 23 m, respectively, from the northern edge of the pond (Figure 7C). At site 1, three cores were collected to a maximum depth (until refusal) of 2.2 meters below the bottom of the pond (Figure 9). At site 2, four cores reached almost 4-meters depth. Adjacent to site 2, three overlapping cores were retrieved to a depth of 3.7 meters. At site 3, closest to the northern shore, five cores were collected to a depth of 4.6 meters below the pond.

Stratigraphy and Chronology

At the three core sites, six main depositional units were identified (Figure 9). Seven out of more than 20 layers due to overwash are identified as likely tsunami deposits. Units C-1 and C-2 are only present at site 2. Unit C-1 is composed of massive silty clay with ostracods, a few cerithids, and two very thin carbonate sand layers near the bottom overlain by a 10-30 cm-thick layer of gray and dark brown, interbedded microbial mats and sand (Figure 9). Unit C-2 (also labeled C-a on Figure 9) consists of mixed green to light-gray medium-grain sand, fragments of microbial mats, silty clay, and organic matter overlain by dark-gray and white massive sand interbedded with fragments of microbial mats. There is a sharp planar contact between C-2 and C-3 above.

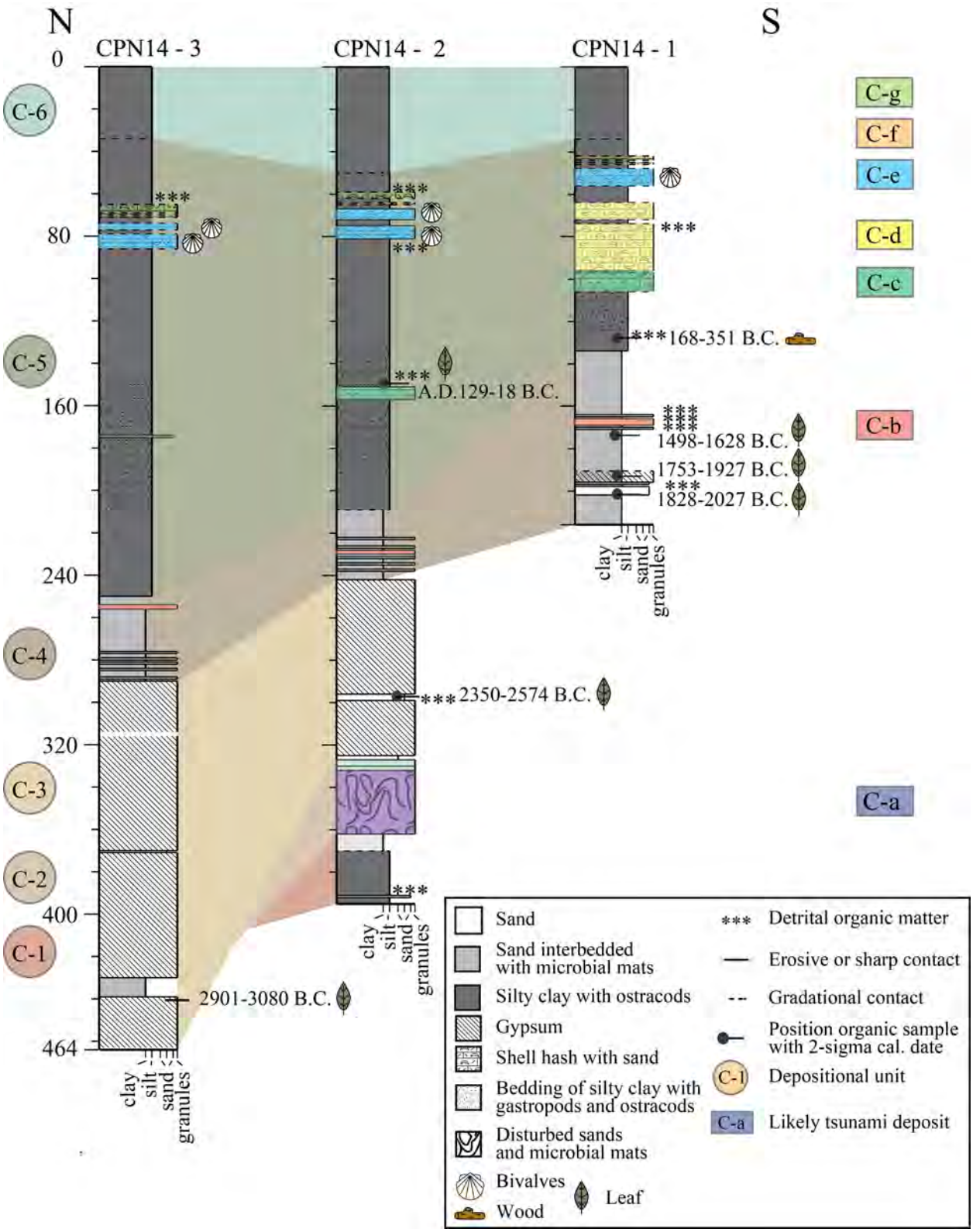

Figure 9. Core logs, radiocarbon date, and stratigraphic interpretation for Cabrita Pond. Cores collected along transect roughly perpendicular to the coast.

Unit C-3, present at sites 2 and 3, is up to 1.6 m thick at site 3 and thins to about 80 cm at site 2. The unit might be present at site 1 but was not reached by the corer. This unit is composed of very pale brown granules of gypsum evaporite interbedded with microbial mats and sand layers with crystals including rose petals and lenticular forms. Near the bottom of site 3, from 430-439 cm depth, laminations of microbial mats are interbedded with carbonate sand and granule-size *Halimeda* fragments. A leaf or piece of charcoal (3A-5L-82) collected at a depth of 440 cm yielded a calibrated date with two ranges of 3080-3070 B.C. and 3025-2901 B.C. Higher in the section at 370 cm depth, a very thin layer of tan, medium-grained sand separates sets of microbial mats; while at 314-316 cm depth, five thin layers of very-well sorted white, fine sands occur within a section of laminated microbial mats. At site 2, a layer of gray fine sand occurs from 296-300 cm depth. A leaf collected at 296 cm from the top of the layer (2A-3B-98) yielded a calendar date with multiple ranges of 2574 -2451 B.C., 2419-2405 B.C., and 2378-2350 B.C. The transition between C-3 and C-4 is marked by an erosive contact.

Present at all three sites, unit C-4, a dark green 28-41 cm thick bed, is composed of laminated microbial mats interbedded with white to light-gray, fine sand, granule-size *Halimeda* segments, lithics, and cemented carbonates. At site 1, the unit includes two gray sand layers each on top of a microbial mat at ~ 196 cm. These sand layers contain abundant microbial mat fragments. A leaf (1A-2B-81.5) collected below the lower sand layer at site 1, yielded a calibrated date with two ranges of 2027-1878 B.C. and 1839-1828 B.C. and provides a close contemporary age for the lower part of unit C-3 and a maximum constraining age for the lower sand layer mixed with microbial mat fragments. Another leaf (1A-2B-74.5) collected above the same lower sand layer yielded a calibrated date between 1927-1753 B.C. and provides a minimum constraining age for the layer. Thus, the lower sand layer with microbial mat fragments was deposited between 2028-1753 B.C. At ~170 cm depth, three distinct layers of *Halimeda* segments are interbedded with sand and microbial mats. All of these layers are interpreted as overwash deposits. One of the *Halimeda* layers is of particular interest because it also contains lithics, microbial mat fragments and gray sand (C-b). At sites 2 and 3, the bottom of unit 4 includes multiple sets (>10) of microbial mats and white sand laminations, with an increase in granule-size *Halimeda* higher in the unit (Figure 9). A layer of *Halimeda* segments interbedded with sand layers and microbial mats occurs at ~230 cm at site 2 and ~256 cm at site 3. These layers are correlated with the three *Halimeda* layers interpreted as an overwash deposit at site 1. A leaf (1A-2B-56.2) collected below the three *Halimeda* layers yielded a calibrated date of 1628-1498 B.C. and provides a close maximum constraining age of 1628 B.C. for the overwash deposit (C-b). A sharp contact and a distinct change in biota marks the boundary between C-4 and C-5.

Unit C-5 is dark-brown silty clay populated with ostracods and interbedded with six bioclastic layers (C-c through C-g; Figure 9). The lowermost bioclastic layer (C-c), a light brown, silty clay sand with cerithids, is observed at all three sites and is thickest at site 1 and thinnest at site 3. Bioclastic layer C-d has a sharp basal contact and is composed of a massive black to gray coarse sand with abundant bivalve, gastropod, ostracod shells, and lithics. This layer is overlain by light brown, silty clay, containing ostracods, organic debris, and small pieces of shell. Higher in the section, layer C-e is a brown to gray, silty clay containing bivalve, gastropod, and ostracod shells as well as a few cemented worm-tube clasts. Bioclastic layers C-f and C-g are both brown silty clay with ostracods and abundant gastropod shells. During the reconnaissance phase of this project, a piece of wood (CPN2-W1-33; Table 2) collected from the mud layer between C-e and C-f yielded a 2-sigma calibrated date with two ranges of A.D. 1445-1524 and A.D. 1558-1631.

Also, a seed (CPN1-W2-28; Table 2) was collected from the same mud layer and yielded a 2-sigma calibrated date with three ranges of A.D. 1647-1687, A.D. 1730-1809, and A.D. 1926-1950. The piece of wood provides close minimum age constraint of A.D. 1631 for C-e. The seed provides close maximum age constraint of A.D. 1647 for C-f. Therefore, C-e was deposited before A.D. 1631 and C-f and C-g were deposited after A.D. 1647.
Unit C-6 is composed of gray silty clay also containing ostracod shells, overlain by brown, silty clay with very thin (1-3 cm) interbeds of ostracod shells, followed by black, organic-rich silty clay with mostly unbroken ostracod shells. Ostracod carapaces of various stages occur throughout the unit, which is thickest at site 2.

Sequence of Pond Environments

Prior to 3000 B.C., Cabrita Pond North appears to have been a shallow muddy pond, very similar to today, characterized by the presence of silt, gastropods, and ostracods. A gradual change in conditions allowed the pond to be populated by microbial mats where low energy and anoxic conditions were prevalent. Shortly before 2900 B.C., Cabrita Pond experienced an energetic event that mixed the sediment and microbial mats, resulting in the formation of layer C-a (Figure 9).

Following that event and perhaps for about 800-900 years, the pond's depositional environment was relatively stable. During the drier months when its water level was lower, the pond was supplied with marine phreatic water that infiltrated through the barrier bar, increasing the pond's salinity and leading to the formation of aragonite, gypsum and halite on the surface of the pond-bottom sediment. During the wetter months, the lake filled with fresh water and a microbial mat grew on top of the evaporate minerals.

From about 2000 B.C. to 500 B.C., it appears that the evaporitic pond was inundated multiple times by seawater, depositing sediment on top of microbial mats and changing the environment to a saline pond. The layers were characterized by carbonate grains and *Halimeda* segments. The most notable of the layers (C-b) was composed of *Halimeda* segments, gray sand, lithics, and microbial mat fragments and was deposited soon after 1628 B.C.

A sharp contact between C-4 and C-5 marks a change in environmental conditions about 500 B.C. At this time, the pond started to receive enough fresh water to maintain an assembly of ostracods and gastropods living in organic silty clay sediments interbedded with sand layers. It is during this time that differences in deposition between the landward and the seaward side of the pond are observed. The landward side is characterized by thick beds of mixed gastropods with lithic material that are absent at sites 2 and 3. Other bioclastic layers are present throughout the unit, hinting to an active period for overwash.

A marked change in biota occurs between units C-5 and C-6. Gastropods and bivalve shells are no longer present in unit C-6, while ostracods become dominate in organic silty clay. In addition, a decrease in the pond's salinity allows for the presence of *Cassiopea sp.* (common name: upside-down jellyfish) to populate the bottom sediment. The pond is typical of a closed lagoon filled with at least 0.5 m deep water all year-round. Therefore, unit C-6 represents a closed coastal lagoon environment, characterized by the accumulation of fine sediment and the presence of benthic ostracods with high amounts of organic matter in the form of peloids. Benthic

ostracods, part of the Class Crustacea, are ubiquitous in most aquatic environments, including coastal lagoons, where they burrow and eat detritus. Growing stages of ostracods take place through molding of their low magnesium calcite carapaces; the presence of carapaces of various stages in the deposit most likely indicates that they are *in situ*.

Overwash Events

Cabrita Pond formed in a recess in the hillslopes of the northeastern coast of the island. Sediment that accumulated in the pond over the past 5,000 years records numerous overwash events. Several of those events appear to be especially energetic, disturbing pond sediment, transporting and depositing carbonate grains, lithic, and *Halimeda* segments into the pond, and changing the pond's environment of deposition. These events are interpreted as tsunamis.

An erosional basal contact and overlying disturbed sediment in unit C-2 records a catastrophic overwash event not long before 2900 B.C. The disturbed sediment is composed of poorly sorted sand and fragments of microbial mats (Figure 9, C-a) and is overlain by two layers of sand containing carbonate fragments separated by pieces of microbial mat. Characteristics of unit C-2 are similar to those found in tsunami deposits in Portugal related to the A.D. 1755 tsunami (Hindson and Andrade, 1999), including a poorly sorted bottom layer attributed deposition under turbulent flow conditions and graded layers on top related to deposition under laminar flow. The following scenario can explain the characteristics of unit C-2: (1) The first wave of a tsunami train eroded the pond-bottom sediment and deposited the lower unit under turbulent flow conditions; (2) as the first wave retreated, it ripped up pieces of the microbial mats and deposited them on the lower sand layer; (3) a second wave inundated the pond and deposited another sandy layer with more organics, followed by a thinner sandy mud cap as fines settled out of the water column. The event also caused a change in the environment of deposition from a saline pond to a hypersaline pond in which more than 100 cm accumulated of evaporites interbedded with microbial mats. The change in environment is also consistent with tsunami inundation.

Unit C-4 records several overwash events between 2000 B.C. to ~500 B.C. The overwash events are represented by layers of *Halimeda* segments and carbonate grains that have an offshore source. One of the layers (C-b) also contained sand, lithics, and microbial mat fragments consistent with tsunami inundation. This event occurred soon after 1628 B.C. The other layers lack variation in composition and are more likely related to less powerful storm surges (Figure 9). Preservation of the overwash deposits in unit C-4 was likely promoted by the presence of microbial mats, particularly at sites 2 and 3.

Unit C-5 records five overwash events since about 500 B.C. The events are represented by layers C-c through C-g and are interpreted as tsunamis (Figure 9). Layer C-c contains gastropods whose lack of color suggests they had been exposed to sunlight for some time, perhaps around the pond's margin, before they were transported and re-deposited in the pond. The absence of lithics in the layer suggests that the wave was not powerful enough to transport sediment from the beach face. Layer C-d, composed of two bioclastic layers of gastropods and lithics separated by silty clay containing organics, represents a significant overwash event. This subunit was recorded only at the landward site. This limited areal distribution is atypical of a tsunami deposit, but its mixed composition, sharp contacts, and mud cap suggest a tsunami origin. Layer C-e, composed of broken shells of the bivalve *Corbula contracta*, marine mollusks and *Cerithidea*

costata, is found at all three core sites. The layer is thickest at site 3, closest to the seashore, where it is composed of two shelly layers with mud and organics on top of each layer. As seen at the other sites, the layers thin landward and only one layer occurs at site 1. Some of the characteristics of this subunit - layers of broken marine bivalves capped by mud and change in its biological assemblage - are more consistent with tsunami inundation than storm surge. This event occurred before A.D. 1631 and might be related to the A.D. 1200-1480 tsunami first reported for Anegada.

Layer C-f and C-g are found at all three sites. The layers are similar in composition, containing ostracods and gastropod shells, thin landward, and were deposited after A.D. 1647. There are several significant events that may have caused overwash at Cabrita Pond in the past ~350 years, including the 1755 Lisbon tsunami, the 1867 Anegada Passage tsunami, and the 1867 hurricane San Narciso. The two layers may be related to two of these three events. The 1755 Lisbon tsunami was reported for several islands in the northeastern Caribbean, probably caused breaches of dunes and widespread deposition of eroded material in salt ponds on Anegada, and may well have caused overwash at Cabrita Pond. The eye of hurricane San Narciso passed ~6 km north of Cabrita Pond, possibly with its upper right quadrant staying offshore (strongest winds). While the hurricane was a category 3, several cays 3 km north and oriented west to east would have served as a breakwater for its storm surge. For the 1867 tsunami, the directionality northward would have allowed for the waves to pass between St. Thomas and St. John to the east, perhaps increasing in height and wrapping around Cabrita Peninsula. In addition, the cays to the north may have reflection the waves back towards St. Thomas. Although additional dating is needed, the preliminary interpretation is that the two layers formed during the 1755 and 1867 tsunamis.

Perseverance Pond

Perseverance Pond is located west of Charlotte Amalie on the southwest coast of St. Thomas (Figure 7A). Historically, there was a sugar cane plantation along the western side of the pond with a road to a dock, which divided the pond in the middle, creating eastern and western ponds. The road between the two ponds is now covered by mangroves. The eastern pond is farther from the historical plantation works and was selected for study. It measures about 60 m across perpendicular to the shoreline and 180 m across parallel to the beach shoreline (Figure 7D). Similar to Cabrita Pond, it is underlain by the Louisenhoj Fm. of Albian age (Donnelly, 1966) and is rimmed by Quaternary deposits vegetated by mangroves and trees. The southern flank of the pond is a barrier bar and beach composed of white carbonate sand, coral fragments, and carbonate rubble. Offshore, the seabed is composed of white carbonate sand on which seagrasses, *Halimeda*, corals, and sponges grow.

Coring

Water depth at the time of coring was 37 cm. During our investigation, a total of 13 cores were collected at three sites along a transect with a bearing of N0.5°E. Site 1 (PERS14-1A), site 2 (PERS14-2A) and site 3 (PERS14-3A) are located 20 m, 32 m, and 50 m, respectively, from the southern edge of the pond. Five cores were collected at site 1, reaching a maximum depth of about 4.1 m below the bottom of the pond. Two cores were collected at site 2, in the middle of the pond, reaching 2.6 m. Four cores were collected at site 3, reaching 3 m below the bottom of

the pond. Two overlapping cores were retrieved adjacent to site 3, reaching 2.1 m below the pond.

Stratigraphy and Chronology

At the three core sites, four main depositional units were identified based on lithostratigraphic and biostratigraphic characteristics (Figure 10). The characteristics of the units are described below. At least eight layers are identified as overwash deposits. Radiocarbon dating of two organic samples collected from the cores provides age constraints for several of the units (Figure 10, Table 3).

Unit P-1, the oldest unit cored, is present at sites 1 and 3. It is characterized by coarse sand (P-a) at the bottom of the unit, only observed at site 3, overlain by a brown massive peat (Figure 10). The coarse sand is composed of abundant granule-size marine shell fragments of various gastropods and bivalve species and some lithic fragments in an organic silty clay matrix. Although its lower contact was not determined, P-a is interpreted as an overwash deposit due to the mixed size and composition of the shell fragments, colorful appearance, and abundance of organic silty clay inside the shells. A distinct and sharp contact, related to an evident change in lithology, separates unit P-1 from P-2.

Unit P-2 is characterized by a green silty clay containing interbeds of sand with ostracods, carbonate grains, foraminifera, and organic material overlain by a light brown massive sandy silty clay with fine roots, scattered *Halimeda* segments, and rip-up clasts. At site 3, where the record is more complete, P-2 contains six interbeds of sand (Figure 10). At sites 1 and 2, the unit contains four and five interbeds of sand, respectively. The lowest sandy layer (P-b) overlies peat and is composed of medium-coarse carbonate sand, abundant organics, and a peat rip-up clast. The uppermost sandy layer (P-c) is composed of sandy silty clay with fine to medium size *Halimeda* segments, fine roots, some organic debris, and few green clay clasts. The four intervening sandy layers are either sandy clay with organic debris or sandy silty clay with fine-grained carbonate fragments and organic debris. A leaf (2A-2L-77) collected towards the bottom of unit P-2 and above layer P-b yielded a calibrated date of 726-720 B.C., 703-695 B.C., and 541-393 B.C. (Figure 10, Table 3). This sample provides a minimum constraining age of 393 B.C. for layer P-b. Another leaf (3A-2B-35.5) in the middle of the section of unit P-2 yielded a calibrated date of A.D. 22-145, A.D. 150-170 and A.D. 194-209. The sample provides a contemporary date for this portion of the deposit and maximum age constraint of A.D. 22 for layer P-c at the top of the unit. A gradational change in lithology and amount of organic debris characterizes the transition from unit P-2 to unit P-3.

Unit P-3 is a red-brown to light brown bioturbated organic-rich sandy silty clay containing carbonates, foraminifera, ostracod shells, and an interlamination of sand composed of carbonate grains, fine-grained size shells, and plant remains (Figure 10). The sand lamination only occurs at site 1 where the unit is thickest. Age constraint for this unit is poor but postdates A.D. 209.

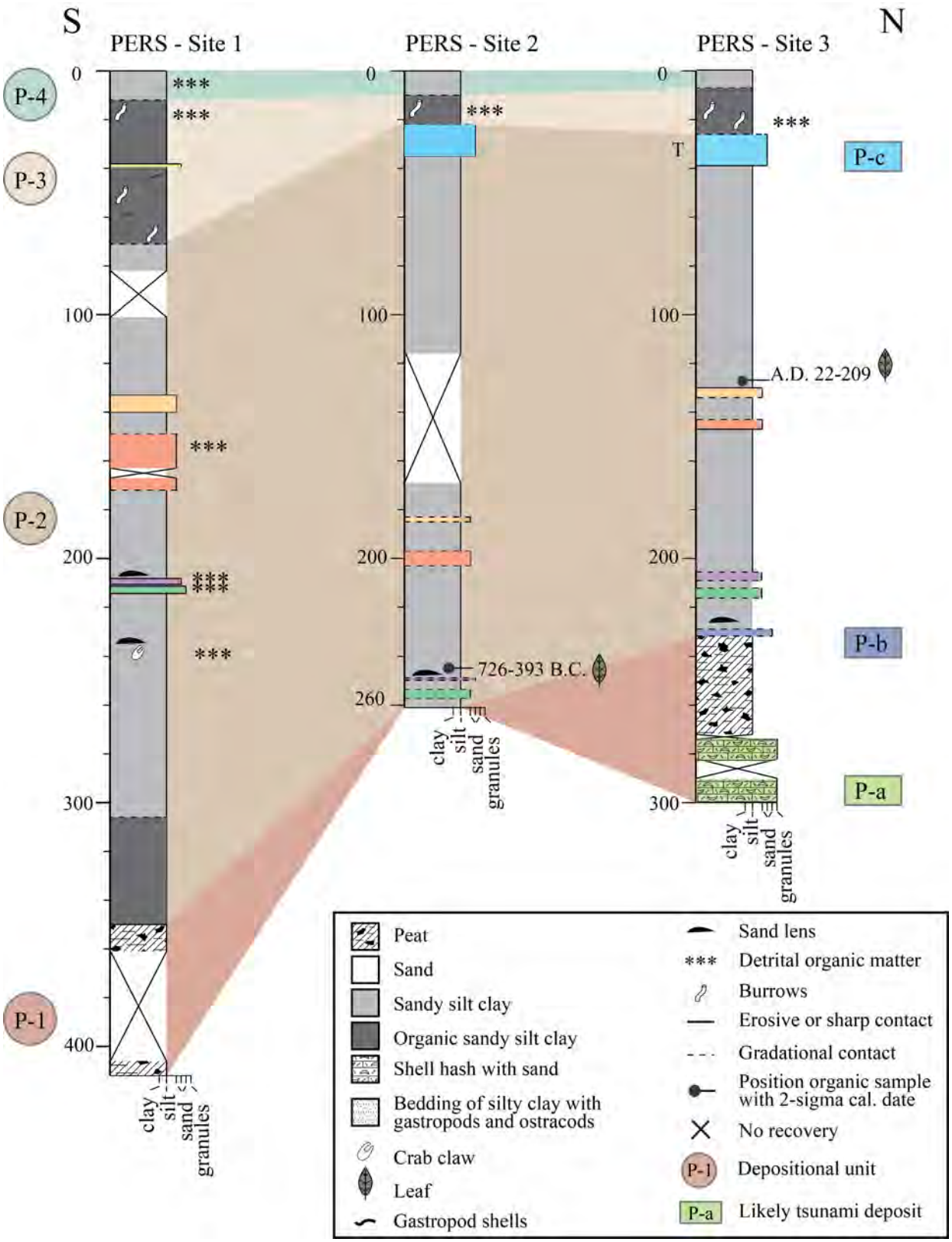

Figure 10. Core logs, radiocarbon date, and stratigraphic interpretation for Perseverance Pond. Cores collected along transect roughly perpendicular to the coast.

Based on the position of the layer within the section, it might have been deposited about 1300-1500 years later. A gradational but distinct contact that has been bioturbated marks a change in composition between units P-3 and P-4. Unit P-4 is brown, sandy silty clay with organic material, silt-size grains of carbonate, diatoms, and foraminifera.

Sequence of Pond Environments

Prior to 726 B.C., Perseverance pond was likely a coastal recess rimmed by mangroves. During the period a high-energy event periodically delivered coarse sand with abundant granule-size marine shell fragments and lithic fragments (P-a) and deposited the sediment on mangrove peat. Not long before 393 B.C., there was a change in environmental conditions that probably resulted from closure of the recess by a barrier bar to form a salt pond. The change in environment was coincident with the deposition of a layer of medium-coarse carbonate sand with abundant organics and a peat rip-up clast (P-b). Subsequent to this change, sandy silty clay accumulated in the pond. Occasionally, overwash deposited sand and organic debris in the pond. After A.D. 22, however, sandy silt clay continues to accumulate with only one sandy layer (P-c) deposited at the very top of the unit. This lack of overwash deposits may be due the inability of storm surge to top the barrier bar at this time or to an increase in fresh water input and bioturbation of the sediment. Unlike the four overwash deposits below, the sandy layer at the top of unit P-2 also contained *Halimeda* segments and clay clasts. The deposition of this layer was also followed by a change to a lower-energy salt-pond environment with a greater input of fresh water in which foraminifera and ostracod thrived and more organics accumulated. Until today, the site continues to be a low-energy salt-water pond environment in which abundant organic material has accumulated and minor bioturbation occurs.

Overwash Events

Eight overwash deposits are identified in Perseverance pond-bottom sediment. Of these overwash deposits three are interpreted as likely tsunami deposits based on the following criteria: mixed composition of sediment derived from multiple environments of deposition, presence of broken shells, rip-up clasts, and mixed or disturbed sediment, and coincidence with changes to the environment of deposition. The deposits that meet some or all of these criteria are layers P-a, P-b and P-c (Figure 10). The other five deposits are likely storm deposits.

Layer P-a is considered a tsunami event due to the coarse and varied nature of its components and high organic content probably due to erosion of underlying peat. Layer P-b is attributed to a tsunami because of the presence of coarse sands and peat rip-up clast and coincidence with a drastic change in environment. Similarly, layer P-c is composed of sand with clay clasts and *Halimeda* segments and is coincident with a change in the environment of deposition.

DISCUSSION

During detailed study of three ponds on the northern and southern coasts of St.Thomas, USVI, a sediment record of overwash events has been uncovered that dates back about 5 kyr (Figure 11). Although some of the overwash deposits are likely to be related to storms, others characterized by inclusion of mixed composition, including sand, lithic, clasts of underlying units, *Halimeda* segments, broken shells and coral fragments, and coincident with changes in the environment of

deposition are interpreted as tsunami deposits. Correlation of likely tsunami deposits from one site to another is tentative, especially for the older deposits. Additional sampling and dating of organic material above and below all the overwash deposits, but especially those interpreted as tsunami deposits, would help to improve age estimates of events and increase confidence in regional correlations.

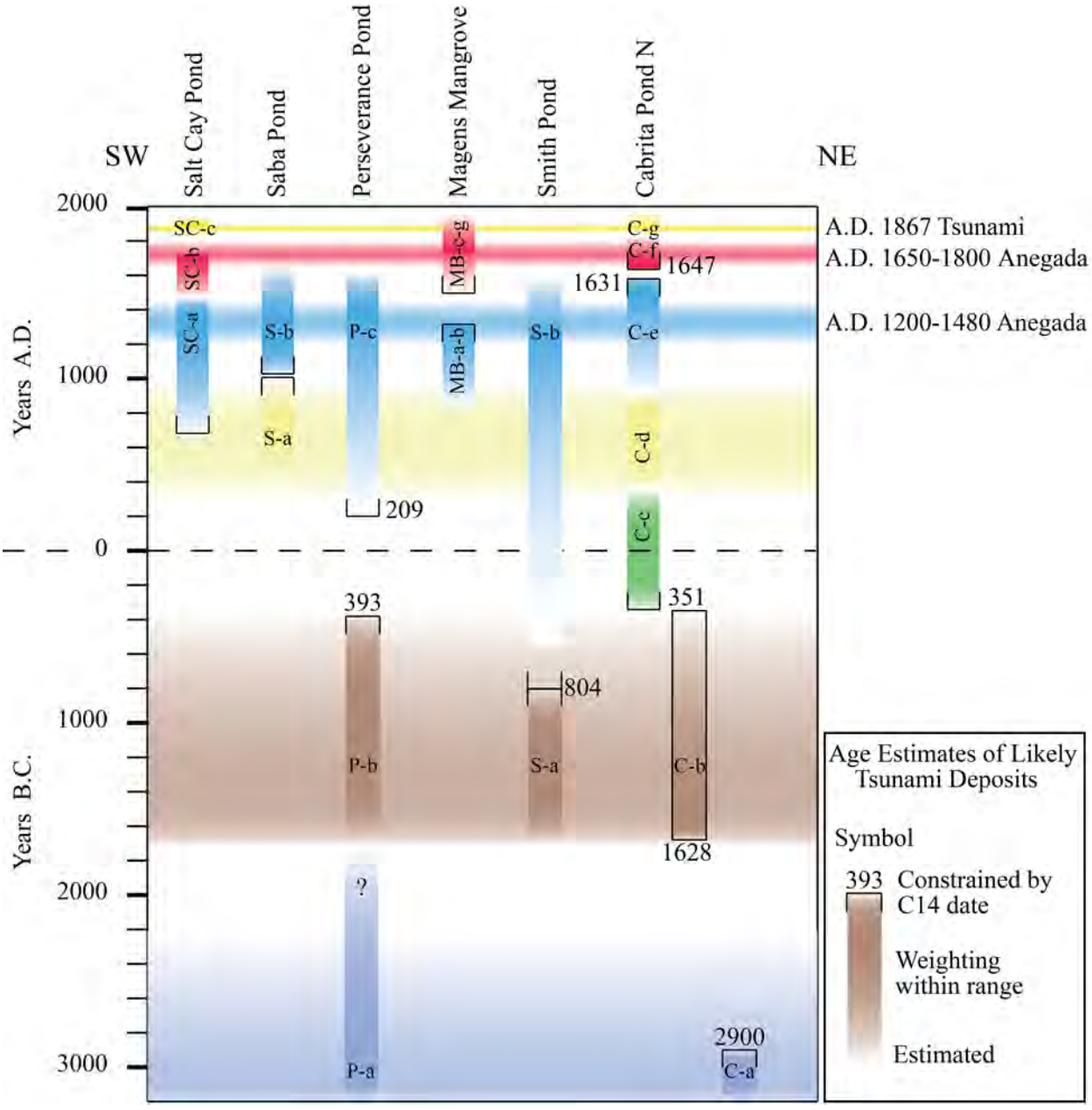

Figure 11. Chronology of overwash deposits likely caused by tsunamis. Age ranges for A.D. 1650-1800 and A.D. 1200-1480 Anegada events are from Atwater et al. (2010 and 2012).

The longest sediment record was recovered from Cabrita Pond North on the northeastern coast of the island. Shortly before 2900 B.C., a catastrophic event caused severe disruption of pond sediment and changed the lagoonal environment to a salt pond. For about 800-900 years, the

pond's depositional environment was relatively stable but slowly became more saline, leading to the formation of aragonite, gypsum and halite on the surface of the pond-bottom sediment. During this period a few sandy overwash layers were deposited in the pond. They are attributed to storms due to the lack of compositional variety and mud caps. From about 2000 B.C. to about 500 B.C., multiple overwash events transported carbonate sand and lithics into the pond. A set of more than 10 white sand laminations interbedded with microbial mats are interpreted as storm deposits due to their composition and frequency. Higher in the unit, sets of laminations of Halimeda fragments are also interpreted as storms deposits. However, a layer containing sand, Halimeda fragments, lithics, and microbial mat fragments is interpreted as a tsunami deposit. This layer formed in what was by then an evaporitic pond soon after 1628 B.C. After about 500 B.C., the pond experienced five overwash events all interpreted to have resulted from tsunamis. These events are represented by layers of coarse lithics, marine shells, gastropods, bivalve shells, and ostracod shells, with some shells broken. In addition, some of the likely tsunami deposits have erosional basal contacts and are capped by mud. The upper three deposits might be related to the A.D. 1200-1480 tsunami first reported for Anegada and thought to have originated in the PRT, the A.D. 1755 Lisbon tsunami reported for several islands in the northeastern Caribbean, and the A.D. 1867 tsunami that originated in Anegada Passage.

At nearby Smith Pond also on the northeastern coast, two overwash events interpreted as tsunamis are recorded in pond-bottom sediment. These events are represented by layers of carbonate sand containing Halimeda segments, foraminifera, and rip-up clasts in one of the layers. The earlier event occurred about 804-899 B.C. The second event may have occurred about 1500-2000 years later and drastically altered the pond's environment. This event might correlate with the A.D. 1200-1480 tsunami or previous event recognized at Cabrita Pond but additional dating of the Smith Pond deposits is needed to confirm either correlation**.**

At Perseverance Pond on the southern coast, pond-bottom sediment records eight overwash events, three of which are interpreted as tsunamis. The earliest event likely occurred before 726 B.C. and is represented by a layer of shelly sand within peat. The second event occurred shortly before 393 B.C. and is represented by medium-coarse carbonate sand with abundant organics and a peat rip-up clast and is coincides with a drastic change in the environment from an open bay to a coastal salt-water pond. The third and latest event occurred after A.D. 22 and perhaps about 1300-1500 years later and changed the pond's environment. This event might correlate also with the A.D. 1200-1480 tsunami but additional dating is needed to constrain the dates of the likely tsunami deposit in the pond sediment. Deposits attributed to this event were recognized at Salt Cay and Saba during the reconnaissance phase of this study.

In tropical regions like the northeastern Caribbean, bioturbation quickly destroys the sediment record unless it is preserved in environments not conducive to biological activity. Therefore, salt ponds are prime targets on both carbonate-platform and volcanic island. The 5 kyr depositional record preserved in ponds on St. Thomas is substantially longer than the 800 yr record in ponds on Anegada, BVI. The longer record on St. Thomas is an advantage to working on steep-sided volcanic islands with salt-water ponds developed in coastal recesses compared to the relatively flat carbonate-platform of Anegada. However, disadvantages of working on a steep-sided volcanic island are high erosion rates and the absence of expansive saline pond areas where tsunamis can deposit broad sheets of sediment 100s to 1000s of meters inland from the shoreline as well as relatively flat low-lying coastal plains on which tsunamis can deposit coral heads and

limestone fragments. Therefore, on St. Thomas, and likely other steep-sided volcanic islands in the Caribbean, the sedimentological history of coastal ponds as well as the characteristics of their deposits must be carefully studied to identify tsunami deposits and to differentiate them from storm deposits that are prevalent in this region.

CONCLUSION

In the PRVI region, the locations and magnitudes of historic earthquakes are poorly constrained and the earthquake potential, maximum magnitude, and recurrence times of most faults zones are essentially unknown (Figure 1). Even if we knew that the PRT had not produced great earthquakes during the historic period, it would not mean that the subduction zone had not produced great earthquakes in the past and would not produce them in the future. A great earthquake produced by faults associated with the PRT would have a major impact on PRVI, especially densely populated San Juan and the northern coast of Puerto Rico, and more distant locations along the U.S. Atlantic coast, including South Carolina, North Carolina, Long Island, New York, Rhode Island, and Massachusetts. Tsunami geology is a powerful tool that can provide critical information about the earthquake potential of the Puerto Rico subduction zone and related faults. Recent investigations on Anegada, BVI (e.g., Atwater et al., 2010 and 2017; Reinhardt et al., 2010) have laid the groundwork for conducting regional paleotsunami studies.

The northeastern Caribbean has been subjected to historical tsunamis from near and distant sources; no doubt it has been subjected to prehistoric tsunamis as well. However, this region is also subject to frequent large storms and hurricanes that produce storm surges that result in overwash of barrier bars and deposition of sediment in coastal ponds. Therefore, care must be taken to distinguish tsunami deposits from storm deposits. In general, tsunami deposits are more broadly distributed than storm deposits in their coastal extent, landward extent, and height above sea level. In the northeastern Caribbean, however, bioturbation in most environments and erosion of steep-sided volcanic islands may have destroyed many tsunami deposits. Those tsunami deposits that remain may be limited to shelly sand layers preserved in salt-water ponds and coral heads and limestone fragments deposited along coasts. For this study focused on pond-bottom sediment, criteria used to identify likely tsunami deposits are mixed composition of sediment derived from multiple environments, presence of broken shells, rip-up clasts, and mixed or disturbed sediment, and coincidence with drastic changes to the environment of deposition.

For the reconnaissance phase of this study, layers composed of shelly sand and Halimeda fragments discovered in coastal ponds on St. Thomas and nearby cays are attributed to five tsunamis (Figures 2 and 6). The uppermost layer at Salt Cay was deposited in the past 300 years and may be related to the 1867 tsunami. Other shelly sand layers at Salt Cay and Cabrita Ponds and Magens Bay mangrove are similar in age to overwash deposits on Anegada that are likely to be related to a tsunami between A.D. 1650-1800. In addition, shelly sand layers at those same locations plus Saba, Perseverance, and Smith Ponds may be related to a tsunami between A.D. 1200-1480 also recognized on Anegada. The event between A.D. 1650-1800 is probably the A.D. 1755 tsunami related to the **M** 8.5 Lisbon earthquake and observed at several islands across the northeastern Caribbean; whereas, the tsunami between A.D. 1200-1480 is thought to have been triggered by a large earthquake associated with the PRT north of Anegada. This study provides further evidence for the A.D. 1650-1800 and A.D. 1200-1480 tsunamis and extends the areas of

impact ~85 km to the southwest into the U.S. Virgin islands and closer to Puerto Rico. Additionally, shelly sand deposits at Saba and Cabrita Ponds are suggestive of two earlier events between 2000-3000+ years ago.

For the detailed investigations at Cabrita, Smith, and Perseverance Ponds, overwash deposits characterized by mixed composition of sand, lithics, clasts of underlying units, *Halimeda* segments, broken shells and coral fragments and coincident with changes in the environment of deposition are attributed to seven tsunamis (Figures 7 and 11). The deposits are thought to be related to two known historical tsunamis and possibly up to five tsunamis during the past 5 kyr. The historical tsunamis that appear to have left their mark in the coastal ponds include the A.D. 1867 tsunami originating in the Anegada Passage and the A.D. 1650-1800 event likely related to the 1755 Lisbon tsunami. The A.D. 1867 and A.D. 1650-1800 tsunamis appear to be represented in the Cabrita Pond sediment record on the northeastern coast but not in the Perseverance Pond record on the southwestern coast. The A.D. 1200-1480 tsunami appears to have inundated all three ponds. Three tsunamis may have inundated the ponds between A.D. 800-1628 B.C. One of those events occurred between 1628-393 B.C. Furthermore, an older event may have disturbed Cabrita Pond, and possibly Perseverance Pond, before 2900 B.C.

Combining the results from reconnaissance and site investigations, a record of the 1867 tsunami has only been found at Salt Cay and Cabrita Pond, whereas, the 1755 trans-oceanic tsunami appears to have been recorded at Salt Cay and Cabrita Ponds as well as Magens Bay mangrove (Figures 2 and 11). The A.D. 1200-1480 event appears to have been recorded at all studied locations, suggesting it had a more significant regional impact than either the 1755 or 1867 events. The tsunami between 1628-393 B.C. was recorded on both coasts suggesting that it may have been similar to the A.D. 1200-1480 event. Although further study is needed to confirm the results of this study and to better constrain the ages of the likely tsunami deposits, the preliminary results suggest that faults associated with the PRT may have produced very large earthquakes and tsunamis twice in the past ~5,000 years.

This study focused on the sedimentary record of coastal ponds and identified overwash deposits that are likely to be related to tsunamis generated by offshore earthquakes. In the future, additional dating of the overwash deposits on St. Thomas as well as documentation of coral heads and other large clasts transported onshore and deposited at higher elevations than the ponds would increase confidence in the tsunami interpretation and correlation of deposits across the island and the region. Further study of pond-bottom sediment on steep-sided volcanic islands as well as coral heads and limestone fragments on flat-lying carbonate-platform islands will likely reveal a more complete history of tsunamis across the northeastern Caribbean. Such a history will help to assess the earthquake and tsunami potential of the PRT as well as other earthquake sources in the region.

ACKNOWLEDGMENTS

Roy Watlington, Emeritus, University of the Virgin Islands, shared his knowledge of history of St. Thomas and seismic and tsunami hazards of the region and facilitated our fieldwork on the island. Carlos Velez and Alex MacKay assisted with surveying of study sites and collecting of cores. Coring of pond sediment was supported by LacCore and laboratory analyses of the cores were conducted at LacCore at the University of Minnesota. In particular, Kristina Brady provided instruction in the use of the coring equipment and Jessica Heck provided guidance in the use of LacCore's laboratory equipment. Fieldwork was also supported by Paul Jobsis, Ian Byrne, and Steve Prosterman of the Center for Marine and Environmental Studies at the University of the Virgin Islands. Steve Prosterman captained marine vessels from the Center and provided safe passage to and from Salt Cay, Saba, and Perseverance Pond. We are grateful to the government official and agencies that permitted work at the study sites, including Hubert Brumant and Robert Moron of the Magens Bay Authority, William Coles of the USVI Department of Natural Resources, and Sean Krigger of VI State Historical Preservation Office. As one of Zamara Fuentes graduate advisors, Brian Atwater provided guidance and review of analyses performed during this project. The views and conclusions presented in this paper are those of the authors and should not be interpreted as necessarily representing the official policies, either expressed or implied, of the U.S. Government.

REFERENCES CITED

Atlantic and Gulf of Mexico Tsunami Hazard Assessment Group, 2008, Evaluation of tsunami sources with the potential to impact the U.S. Atlantic and Gulf Coasts - A report to the Nuclear Regulatory Commission, U.S. Geological Survey Administrative Report, 322 p.

Atwater, B. F., ten Brink, U. S., Buckley, M., Halley, R. S., Jaffe, B. E., López-Venegas, A. M., Reinhardt, E. G., Tuttle, M. P., Watt, S., and Wei, Y., 2010, Geomorphic and stratigraphic evidence for an unusual tsunami or storm a few centuries ago at Anegada, British Virgin Islands, Natural Hazards, v. 63, no. 1, p. 51-84.

Atwater, B. F., Fuentes, Z., Halley, R. B., Ten Brink, U. S., and Tuttle, M. P., 2014, Effects of 2010 Hurricane Earl amidst geologic evidence for greater overwash at Anegada, British Virgin Islands, Advances in Geosciences, v. 38, p. 21-30.

Atwater, B. F., ten Brink, U., Cescon, A. L., Feuillet, N., Fuentes, Z., Halley, R. B., Nuñez, C., Reinhardt, E. G., Roger, J., Sawai, Y., Spiske, M., Tuttle, M., Wei, Y., and Accardo, J., 2017, Extreme waves in the British Virgin Islands during the last centuries before 1500 CE, Geosphere, v. 13, p. 301-368

Atwater, B. F., ten Brink, U. S., Cescon, A. L., Feuillet, N., Fuentes, Z., Halley, R. B., Nuñez, C., E.

Reinhardt, G., Roger, J. H., Sawai, Y., Spiske, M., Tuttle, M. P., Wei, Y., and Weil-Accardo, J. 2017. Extreme waves in the British Virgin Islands during the last centuries before 1500 CE, Geosphere, v. 13, p. 301-368.

Bondevik, S., Mangerud, J., Dawson, S., Dawson, A., and Lohne, Ø., 2005, Evidence for three North Sea tsunamis at the Shetland Islands between 8000 and 1500 years ago: Quaternary Science Reviews, v. 24, no. 14-15, p. 1757-1775.

Brooks, G. R., Larson, R. A., Devine, B., and Schwing, P. T., 2015, Annual to millennial record of sediment delivery to US Virgin Island coastal environments, The Holocene, v. 25, p. 1015-1026.

Cangialosi, J. P., 2011, Tropical Cyclone Report Hurricane Earl, NOAA, 1-29.
Deng and Sykes, L., 1995, Determination of euler poles for Caribbean- North American plate using slip vectors of interplate earthquakes, Tectonics, v. 14, p. 39-53.
Dixon, T., Farina, F., DeMets, C., Jansma, P., Mann, P., and Calais, E., 1998, Relative motion between the Caribbean North American plates and related boundary zone deformation based on a decade of GPS observations, J. Geophys. Res., v. 103, p. 15157-15182.
Donnelly, T. W., 1966, Geology of St. Thomas and St. John, U. S. Virgin Islands, Geological Society of America Memoirs, v. 98, p. 85-177.
Donnelly, J. P., 2005, Evidence of past intense tropical cyclones from backbarrier salt pond sediments: a case study from Isla de Culebrita, Puerto Rico, USA, Journal of Coastal Research, v. 42, p. 201–210.
Goff, J., McFadgen, B. G., and Chague-Goff, C., 2004, Sedimentary differences between the 2002 Easter storm and the 15th-century Okoropunga tsunami, southeastern North Island, New Zealand, Marine Geology, v. 204, no. 1-2, p. 235-250.
Goto, K., Chagué-Goff, C., Fujino, S., Goff, J., Jaffe, B., Nishimura, Y., Richmond, B., Sugawara, D., Szczuciński, W., Tappin, D. R., Witter, R. C., and Yulianto, E., 2011, New insights of tsunami hazard from the 2011 Tohoku-oki event, Marine Geology, v. 290, p. 46-50.
Heiri, O., Lotter, A. F., and Lemcke, G., 2001, Loss on ignition as a method for estimating organic and carbonate content in sediments, reproducibility and comparability of results Journal of Paleolimnology, v. 25, no. 1, p. 101-110.
Hindson, R. A., and Andrade, C., 1999, Sedimentation and hydrodynamic processes associated with the tsunami generated by the 1755 Lisbon earthquake, Quaternary International, v. 56, no. 1, p. 27-38.
Jaffe, B. E., Borrero, J. C., Prasetya, G. S., Peters, R., McAdoo, B., Gelfenbaum, G., Morton, R., Ruggiero, P., Higman, B., Dengler, L., Hidayat, R., Kingsley, E., Kongko, W., Lukijanto, Moore, A., Titov, V., and Yulianto, E., 2006, Northwest Sumatra and Offshore Islands Field Survey after the December 2004 Indian Ocean Tsunami, Earthquake Spectra, v. 22 p. 105-135.
Jankaew, K., Atwater, B.F., Sawai, Y., Choowong, M., Charoentitirat, T., and Martin, M.E., 2008, Ancestral tsunamis in Thailand, Nature, v. 455, p. 1228-1231.
Jansma, P. E., Mattioli, G. S., Lopez, A., DeMets, C., Dixon, T. H., Mann, P., and Calais, E., 2000, Noetectonics of Puerto Rico and the Virgin Islands, northeastern Caribbean, from GPS geodesy, Tectonics, v. 6, p. 1021-1037.
Kelts, K. R., 2003, Components in lake sediments, *in* Valero Garcés, B. L., ed., Limneology in Spain: A tribute to Kerry Kelts, Madrid, Consejo Superior de Investigaciones Cientificas, p. 59-72.
Kennedy, A. B., Mori, N., Zhang, Y., Yasuda, T., Chen, S.-E., Tajima, Y., Pecor, W., and Toride, K., 2016, Observations and Modeling of Coastal Boulder Transport and Loading During Super Typhoon Haiyan, Coastal Engineering Journal, v. 58 p.1-25.
Lopez, A., Jansma, P., Calais, E., Demets, C., Dixon, T., Mann, P., and Mattioli, G., 1999, Microplate tectonics along the North American-Caribbean plate boundary: GPS geodetic constraints on rigidity of the Puerto Rico-Northern Virgin Islands (PRVI) block, convergence across the Muertos Trough, and extension in the Mona Canyon, Eos, Trans. AGU, v. 82, p. S77.
Lopez, A. M., 2006, Is there a northern Lesser Antilles forearc block?, Geophysical Research Letters, v. 33. Doi: 10.1029/2005GL025293.
Mann, P., Schubert, C., and Burke, K., 1990, Review of Caribbean neotectonics. *In* G. Dengo and J.E. Case (editors), The Geology of North America, v. H, The Caribbean Region. Geol. Soc. Am., Boulder, CO, p. 307-337.

Mann, P., Calais, E., Ruegg, J.-C., DeMets C., Jansma, P.E., and Mattioli, G.S., 2002, Oblique collision in the northeastern Caribbean from GPS measurements and geological observations, Tectonics, v. 21, n. 6. p. 1057.
Masson, D. G. and Scanlon, K. M., 1991, The neotectonic setting of Puerto Rico, Geological Society of America Bulletin, v. 103, p. 144-154.
McCann, W. R., 1985, On the earthquake hazards of Puerto Rico and the Virgin Islands, Seismological Society of America Bulletin, v. 75, p. 251-262.
Minoura, K., Imamura, F., Sugawara, D., Kono, Y., and Iwashita, T., 2001, The 869 Jogan tsunami deposit and recurrence interval of large-scale tsunami on the Pacific coast of northeast, Japan, Journal of Natural Disaster Science, v. 23, p. 83-88.
Morton, R. A., Richmond, B., Jaffe, B.E., and Gelfenbaum, G., 2006, Reconnaissance investigation of Caribbean extreme wave deposits-Preliminary observations, interpretations, and research directions, U.S. Geological Survey Open-File Report 2006-1293, p. 1-46.
Morton, R. A., Goff, J. R., and Nichol, S. L., 2007, Impacts of the 2004 Indian ocean tsunami on the southwest coasts of Sri Lanka, Coastal Sediments, p. 1-14.
Moya, J. C., and Mercado, A., 2006, Geomorphologic and stratigraphic investigations on historic and pre-historic tsunami in northwestern Puerto Rico: Implications for long term coastal evolution, in Caribbean tsunami hazard A. Mercado-Irizarry and L. P. (Editors), World Scientific Publishing, p. 149-177.
Mueller, C. S., Frankel, A. D., Petersen, M. D., and Leyendecker, E. V., 2003, Documentation for 2003 USGS seismic hazard maps of Puerto Rico and the U.S. Virgin Islands, U.S. Geological Survey, Golden, Colorado, Open file report 03-379.
Nanayama, F., Shigeno, K., Satake, K., Shimokawa, K., Koitabashi, K., Miyasaka, S., and Ishii, M., 2000, Sedimentary differences between the 1993 Hokkaido-nansei-oki tsunami and the 1959 Miyakojima typhoon at Taisei, southwestern Hokkaido, northern Japan, Sedimentary Geology, v. 135, p. 255-264.
Namegaya, Y., and Satake, K., 2014, Reexamination of the A.D. 869 Jogan earthquake size from tsunami deposit distribution, simulated flow depth, and velocity, Geophysical Research Letters v. 41, n. 7, p. 2297-2303, doi:10.1002/2013GL058678.
Nelson, A. R., Briggs, R. W., Dura, T., Engelhart, S. E., Gelfenbaum, G., Bradley, L.-A., Forman, S. L., Vane, C. H., and Kelley, K. A., 2015, Tsunami recurrence in the eastern Alaska-Aleutian arc: A Holocene stratigraphic record from Chirikof Island, Alaska, Geosphere v. 11, p. 1-34.
Peters, R., and B. E. Jaffe, 2010, Identification of tsunami deposits in the geologic record; developing criteria using recent tsunami deposits, U. S. Geological Survey Open-File Report 2010-1239, 39 p. [http://pubs.usgs.gov/of/2010/1239/].
Pilarczyk, J. E., and Reinhardt, E. G., 2011, Homotrema rubrum (Lamarck) taphonomy as an overwash indicator in Marine Ponds on Anegada, British Virgin Islands. Natural Hazards, v. 63, n. 1, p. 85-100, doi:10.1007/s11069-010-9706-3.
Pilarczyk, J. E., Horton, B. P., Soria, J. L. A., Switzer, A. D., Siringan, F., Fritz, H. M., Khan, N. S., Ildefonso, S., Doctor, A. A., and Garcia, M. L., 2016, Micropaleontology of the 2013 Typhoon Haiyan overwash sediments from the Leyte Gulf, Philippines: Sedimentary Geology, v. 339, p. 104-114.
Prentice, C. and Mann, P., 2005, Paleoseismic study of the south Lajas fault: First documentation of an onshore Holocene fault in Puerto Rico, P. Mann ed., GSA Special Paper 385, Active tectonics and seismic hazards of PR, the Virgin Islands, and offshore areas, p. 215-222.
Reicherter, K., Vonberg, D., Koster, B., Fernández-Steeger, T., Grützner, C., and Mathes-Schmidt, M., 2010, The sedimentary inventory of tsunamis along the southern Gulf of Cádiz

(southwestern Spain), Zeitschrift für Geomorphologie, Supplementary Issue v. 54, n. 3, p. 147-173.
Reid, H., and Taber, S., 1919, The Puerto Rico earthquakes of October-November 1918, Bulletin of the Seismological Society of America, v. 9, p. 95-127.
Reinhardt, E., Pilarczyk, J., and Brown, A., 2012, Probable tsunami origin for a Shell and Sand Sheet from marine ponds on Anegada, British Virgin Islands, Natural Hazards, v. 63, n. 1, p. 101-117, doi:10.1007/s11069-011-9730-y.
Schnurrenberger, D., Russell, J., and Kelts, K., 2003, Classification of lacustrine sediments based on sedimentary components, Journal of Paleolimnology, v. 29, p. 141-154.
Soria, J. L. A., Switzer, A. D., Villanoy, C. L., Fritz, H. M., Bilgera, P. H. T., Cabrera, O. C., Siringan, F. P., Maria, Y. Y.-S., Ramos, R. D., and Fernandez, I. Q., 2016, Repeat Storm Surge Disasters of Typhoon Haiyan and Its 1897 Predecessor in the Philippines: Bulletin of the American Meteorological Society, v. 97, no. 1, p. 31-48.
Sperazza, M., Moore, J. N., and Hendrix, M. S., 2004, High-Resolution Particle Size Analysis of Naturally Occurring Very Fine-Grained Sediment Through Laser Diffractometry, Journal of Sedimentary Research, v. 74, no. 5, p. 736-743.
Spiske, M., and Halley, R. B., 2014, A coral-rubble ridge as evidence for hurricane overwash, Anegada (British Virgin Islands), Advances in Geosciences v. 38, p. 9-20.
Stuvier, M., P. J. Reimer, and R. W. Reimer (2017). CALIB 7.1 [WWW program] at http://calib.org, accessed 2017-1-18.
Sykes, L. R., McCann, W. R., and Kafka, A. L., 1982, Motion of Caribbean plate during last 7 million years and implications for earlier Cenozoic movements, Journal of Geophysical Research, v. 87, p. 10656-10676.
Spiske, M., and Halley, R. B., 2014, A coral-rubble ridge as evidence for hurricane overwash, Anegada (British Virgin Islands), Advances in Geosciences v. 38, p. 9-20.
Tuttle, M. P., Ruffman, A., Anderson, T., and Jeter, H., 2004, Distinguishing tsunami from storm deposits in Eastern North America; the 1929 Grand Banks tsunami versus the 1991 Halloween storm, Seismological Research Letters, v. 75, no. 1, p. 117-131.
van Gestel, J.-P., P. Mann, J. F. Dolan, and N. R. Grindlay.,1998, Structure and tectonics of the upper Cenozoic Puerto Rico-Virgin Islands carbonate platform as determined from seismic reflection studies, J. Geophys. Res., v. 103, n. B12, p. 30505–30530, doi:10.1029/98JB02341.
Wei, Y., ten Brink, U., Atwater, B. F., Tuttle, M. P., Halley, R. B., Feuillet, N., Accardo Accardo, J., and Fuentes, Z., 2012, Near-field tsunami inferred from numerical modeling of medieval overwash at Anegada, British Virgin Islands, Fall Meeting, AGU, San Francisco, California.
Wright, H. E., Jr., 1991, Coring tips, Journal of Paleolimnology, v. 6, no. 1, p. 37-49.
Wright, H. E. J., 1967, A square-rod piston sampler for lake sediments, Limnological Research Center University of Minnesota, p. 975-976.
Woodruff, J. D., Donnelly, J. P., Mohrig, D., and Geyer, W. R., 2008, Reconstructing relative flooding intensities responsible for hurricane-induced deposits from Laguna Playa Grande, Vieques, Puerto Rico. Geology, v. 36, p. 391-394. Doi:10.1130/G24731A.1.
Zahibo, N., Pelinovsky, E., Yalciner, A. C., Kurkin, A., Koselkov, A., and Zaitsev, A., 2003, The 1867 Virgin Island Tsunami, Natural Hazards and Earth System Sciences, v. 3, p. 367-376.

BIBLIOGRAPHY OF RELATED PUBLICATIONS

Fuentes, Z., Tuttle, M., and Schmidt, W., 2012, Overwash deposits from the past 3,000 years on St. Thomas, U.S. Virgin Islands, Geological Society of America, Abstracts with Programs, v. 42, n. 5, p. 460.

Fuentes, Z., Tuttle, M. P., and W. E. S., 2016, Ecological changes and overwash events at three coastal ponds of St. Thomas, U.S. Virgin Islands, in Proceedings II General Assembly of the Latin America and Caribbean Seismological Commission (LACSC), San José, Costa Rica.

Fuentes, Z., Tuttle, M., and Schmidt, W., 2017, Sand scripts of past tsunamis in coastal ponds of St. Thomas, U.S. Virgin Islands, Seismological Research Letters-Eastern Section, *accepted*.

Fuentes, Z., Tuttle, M. P., and Schmidt, W. E., 2017, Ecological changes and overwash deposits at three coastal ponds on St. Thomas, U.S. Virgin Islands, *in revision*.